

Non-minimal UED confronts $B_s \rightarrow \mu^+ \mu^-$

Anindya Datta ^{*}, Avirup Shaw [†]

*Department of Physics, University of Calcutta, 92 Acharya Prafulla Chandra Road,
Kolkata 700009, India*

Abstract

Addition of boundary localised kinetic and Yukawa terms to the action of a 5-dimensional Standard Model would non-trivially modify the Kaluza-Klein spectra and some of the interactions among the Kaluza-Klein excitations compared to the minimal version of this model, in which, these boundary terms are not present. In the minimal version of this framework known as Universal Extra Dimensional model, special assumptions are made about these unknown, beyond the cut-off contributions to restrict the number of unknown parameters of the theory to a minimal. We estimate the contribution of Kaluza-Klein modes to the branching ratios of $B_{s(d)} \rightarrow \mu^+ \mu^-$ in the framework of non-minimal Universal Extra Dimensional, at one loop level. The results have been compared to the experimental data to constrain the parameters of this model. From the measured decay branching ratio of $B_s \rightarrow \mu^+ \mu^-$ (depending on the values of boundary localised parameters) lower limit on R^{-1} can be as high as 800 GeV. We have briefly reviewed the bounds on nmUED parameter space coming from electroweak precision observables. The present analysis ($B_s \rightarrow \mu^+ \mu^-$) has ruled out new regions of parameter space in comparison to the analysis of electroweak data. We have revisited the bound on R^{-1} in Universal Extra Dimensional model, which came out to be 454 GeV. This limit on R^{-1} in Universal Extra Dimensional framework is not as competitive as the limits derived from the consideration of relic density or Standard Model Higgs boson production and decay to $W^+ W^-$. Unfortunately, $B_d \rightarrow \mu^+ \mu^-$ decay branching ratio would not set any significant limit on R^{-1} in a minimal or non-minimal Universal Extra Dimensional model.

PACS No: 11.10 Kk, 12.60.-i, 14.70.Hp, 14.80.Rt

I Introduction

After the discovery of the Higgs boson at the LHC experiment, the new challenge to particle physics is to provide a framework in which there exists a natural Dark Matter (DM) candidate, as the Standard Model (SM) itself does not have a sufficiently massive weakly interacting particle to be a good candidate for DM. Thus one is compelled to look beyond the SM and in this endeavour, extra dimensional scenarios offer such a paradigm. Some of the variants of extra dimensional theories offer the solution to the DM [1, 2] puzzle along with many others like gauge

^{*}email: adphys@caluniv.ac.in

[†]email: avirup.cu@gmail.com

coupling unifications [3] and fermion mass hierarchy [4] to name a few. A particular extension of the SM needs special attention in this regard. This is known as Universal Extra Dimensional (UED) Model where all the SM fields can propagate in 4+1 dimensional space-time. The extra dimension (say, y) is compactified on a circle (S^1) of radius R [5]. 5-dimensional (5-D) action, which has the same field content as the SM, would respect the same $SU(3)_c \times SU(2)_L \times U(1)_Y$ gauge symmetry. The 4-dimensional (4-D) effective theory is characterised by Kaluza-Klein (KK) towers corresponding to each SM field. The mass of a n^{th} KK-mode excitation is given by $m_n^2 = m^2 + \frac{n^2}{R^2}$; n being the KK-number which is nothing but the discretized momentum in y -direction and m is the 0-mode mass. SM particles have been identified with the $n = 0$ mode fields in the effective theory. However there is one caveat, unlike the SM, the 0-mode fermions in the effective theory are not chiral, but are vector like in nature. To get rid of the unwanted fermion 0-modes, one needs to impose an extra Z_2 symmetry: $y \rightarrow -y$ on the action. Fields which do not have 0-modes are chosen to be odd under this Z_2 symmetry. Rest of the fields, having 0-modes, are even under this discrete transformation. The space of y is restricted from 0 to πR and is called an S^1/Z_2 orbifold. Two boundary points of the orbifold are also called the fixed points as they transform onto themselves under this Z_2 transformation.

Radiative correction plays [6, 7] an important role to cure a highly degenerate KK-mass spectrum in this model. These corrections fall into two categories: namely the finite bulk corrections and more importantly the boundary localised corrections having logarithmic dependence on the cut-off scale Λ . A very special assumption is being taken in minimal UED (mUED) which ensures vanishing radiative corrections at the scale Λ . In a more general scenario like non-minimal UED (nmUED) [8]-[14], this special assumption is being avoided. Instead, one assumes the boundary localised corrections as free parameters of the model. In this article, phenomenology of a particular non-minimal scenario in which kinetic and Yukawa terms involving fields are added to the 5-D action, at boundary points, will be investigated. Coefficients of boundary localised kinetic terms (BLKT) and boundary localised Yukawa terms (BLYT) along with the radius of compactification, R can be chosen as free parameters and experimental data can be used to constrain them.

Various phenomenological studies in the framework of nmUED have been made to constrain non-minimality parameters from the perspective of electroweak observables [13], S, T and U parameters [11, 15], relic density [16, 17], measurement of decay width of Z -boson to a pair of b -quarks [18], SM Higgs boson production and decay [19] and from the LHC experiments [20, 21].

Historically any search of *new physics* beyond the SM has been guided by the effects like precision electroweak variables like ρ (T)-parameter, R_b (Z -boson decay width to a pair of b quarks normalised to total hadronic decay width), A_{FB}^b (forward-backward asymmetry of b quarks at Z -pole) etc. Incidentally, all of these electroweak observables are extremely sensitive to the quantum corrections. Furthermore, large top quark mass plays a crucial role to amplify these quantum effects. In the same spirit, we would like to investigate how a precisely measured quantity namely, branching ratio of $B_{s(d)}$ meson decay to $\mu^+\mu^-$ could help us in this endeavour. Recent experimental measurement of these branching ratios by CMS [22] and LHCb [23] collaborations have created some excitements among the high energy physics community, as the

$B_s \rightarrow \mu^+ \mu^-$ decay has been thought to be one of the harbingers of new physics. Unfortunately, the measured value of the branching ratio is more or less consistent with the SM prediction [24]. There exists only a one (two)-standard deviation difference between the experimentally measured value and the SM estimation of the B_s (B_d) branching ratio to $\mu^+ \mu^-$ pair. However, this close agreement of experiment with the SM, can be exploited to constrain the parameters of any BSM scenario. In this article we will be performing such an exercise. We will evaluate the $Br(B_{s(d)} \rightarrow \mu^+ \mu^-)$ in nmUED framework and compare our results with that from the experiment.

$Br(B_{s(d)} \rightarrow \mu^+ \mu^-)$ in the framework of UED has been previously estimated in ref. [25]. However, presence of boundary localised terms (BLT) in the action would non-trivially change masses of KK-excitations and some of the couplings involving KK-excitations in nmUED framework. Thus it would not be a trivial rescaling of an earlier calculation [25] of $B_{s(d)} \rightarrow \mu^+ \mu^-$. To the best of our knowledge, this is the first estimation of $B_{s(d)}$ branching ratios in the framework of nmUED.

In the following section, we will evaluate relevant interactions and vertices in the framework of KK-parity-conserving nmUED with a brief introduction of the model. In section 3 and 4 we will present some calculational details and numerical results respectively. The electroweak precision variables have been always very effective in constraining any form of new physics. We will briefly review the effect of precision observables (namely the S , T and U) on the nmUED parameter space at the end. We conclude in section 5.

II A lightning review of KK-parity-conserving nmUED scenario

In this section, we discuss the KK-parity conserving nmUED model in brief, with focus on the interactions necessary for our calculations. We will need gauge and Yukawa interactions of the fermion KK-modes. Furthermore, we will briefly touch the spectrum of Goldstone bosons and physical scalars as they play an important role in our analysis as we proceed to present a one loop calculation done in Feynman gauge, which is characterised by the presence of unphysical degrees of freedom in the particle spectra.

Let us start with the 5-D fermionic action with BLKT [12, 14]:

$$S_{fermion} = \int d^5x \left[\bar{\Psi}_L i \Gamma^M D_M \Psi_L + r_f \{ \delta(y) + \delta(y - \pi R) \} \bar{\Psi}_L i \gamma^\mu D_\mu P_L \Psi_L + \bar{\Psi}_R i \Gamma^M D_M \Psi_R + r_f \{ \delta(y) + \delta(y - \pi R) \} \bar{\Psi}_R i \gamma^\mu D_\mu P_R \Psi_R \right]. \quad (1)$$

In 5-dimensions four component Dirac spinors $\Psi_L(x, y)$ and $\Psi_R(x, y)$ can be written in terms of two component spinors [12, 14]:

$$\Psi_L(x, y) = \begin{pmatrix} \phi_L(x, y) \\ \chi_L(x, y) \end{pmatrix} = \sum_n \begin{pmatrix} \phi_L^{(n)}(x) f_L^n(y) \\ \chi_L^{(n)}(x) g_L^n(y) \end{pmatrix}, \quad (2)$$

$$\Psi_R(x, y) = \begin{pmatrix} \phi_R(x, y) \\ \chi_R(x, y) \end{pmatrix} = \sum_n \begin{pmatrix} \phi_R^{(n)}(x) f_R^n(y) \\ \chi_R^{(n)}(x) g_R^n(y) \end{pmatrix}. \quad (3)$$

Γ -matrices satisfy Clifford algebra in 4+1 dimensions: $\{\Gamma_M, \Gamma_N\} = 2g_{MN}$, where $(M, N = 0, \dots, 4)$ ¹ with the metric $g_{MN} \equiv \text{diag}(1, -1, -1, -1, -1)$. The Γ matrices are defined as $\Gamma^M \equiv \{\gamma^\mu, i\gamma^5\}$, with $(\mu = 0, \dots, 3)$. The 5-D covariant derivative is defined as $D_M \equiv \partial_M + ig_2^5 \frac{\sigma^a}{2} W_M^a + ig_1^5 \frac{Y}{2} B_M$, with g_2^5 and g_1^5 are the respective 5-D $SU(2)_L$ and $U(1)_Y$ gauge coupling constants. $\frac{\sigma^a}{2}$ and $\frac{Y}{2}$ are the corresponding generators.

Strength of the BLKT for the fermion fields is parametrised by r_f which we choose to be the same for Ψ_L and Ψ_R to respect the *chiral symmetry*. We choose equal strengths of the boundary terms at the fixed points ($y = 0$ and $y = \pi R$) which leads to KK-parity² conserving interactions. We will stick to this convention while defining the gauge and Yukawa interactions in the following. However, in general one can adopt asymmetric boundary terms leading to non-conservation of KK-parity. Phenomenology of such KK-parity-non-conserving scenario can be found in [14, 21].

One can easily obtain the equation of motion governing the dynamics of $f_{L(R)}$ and $g_{L(R)}$ from the above action. With appropriate boundary conditions, solutions are as the following [9, 13, 17]:

$$f_L^n = g_R^n = N_n^f \begin{cases} \frac{\cos \left[m_{f^{(n)}} \left(y - \frac{\pi R}{2} \right) \right]}{\cos \left[\frac{m_{f^{(n)}} \pi R}{2} \right]} & \text{for } n \text{ even,} \\ -\frac{\sin \left[m_{f^{(n)}} \left(y - \frac{\pi R}{2} \right) \right]}{\sin \left[\frac{m_{f^{(n)}} \pi R}{2} \right]} & \text{for } n \text{ odd,} \end{cases} \quad (4)$$

and

$$g_L^n = -f_R^n = N_n^f \begin{cases} \frac{\sin \left[m_{f^{(n)}} \left(y - \frac{\pi R}{2} \right) \right]}{\cos \left[\frac{m_{f^{(n)}} \pi R}{2} \right]} & \text{for } n \text{ even,} \\ \frac{\cos \left[m_{f^{(n)}} \left(y - \frac{\pi R}{2} \right) \right]}{\sin \left[\frac{m_{f^{(n)}} \pi R}{2} \right]} & \text{for } n \text{ odd.} \end{cases} \quad (5)$$

N_n^f , being the normalisation for n^{th} KK-mode, could be determined from orthonormality conditions:

$$\left. \begin{aligned} \int_0^{\pi R} dy [1 + r_f \{\delta(y) + \delta(y - \pi R)\}] f_L^m f_L^n \\ \int_0^{\pi R} dy [1 + r_f \{\delta(y) + \delta(y - \pi R)\}] g_R^m g_R^n \end{aligned} \right\} = \delta^{nm}; \quad \left. \begin{aligned} \int_0^{\pi R} dy f_R^m f_R^n \\ \int_0^{\pi R} dy g_L^m g_L^n \end{aligned} \right\} = \delta^{nm}, \quad (6)$$

¹ $M, N = 4$ corresponds to the y -direction in space.

²After restricting the y -direction between 0 and πR and imposing a discrete Z_2 symmetry on the action the residual symmetry of the action is a reflection symmetry along the line $y = \frac{\pi R}{2}$. The transformation of KK-excitations under this reflection is characterised by KK-parity. An immediate consequence of KK-parity conservation is, in any interaction vertex involving KK-excitations, the sum of KK-numbers must be an even integer.

and it takes the form:

$$N_n^f = \sqrt{\frac{2}{\pi R}} \left[\frac{1}{\sqrt{1 + \frac{r_f^2 m_{f(n)}^2}{4} + \frac{r_f}{\pi R}}} \right]. \quad (7)$$

$m_{f(n)}$ is the n^{th} KK-mode solution of the following transcendental equations [9, 17]:

$$\frac{r_f m_{f(n)}}{2} = \begin{cases} -\tan\left(\frac{m_{f(n)} \pi R}{2}\right) & \text{for } n \text{ even,} \\ \cot\left(\frac{m_{f(n)} \pi R}{2}\right) & \text{for } n \text{ odd.} \end{cases} \quad (8)$$

We would like to focus on the other relevant interactions (gauge, scalar and Yukawa) which are also important for our discussion [13, 18]:

$$S_{gauge}^W = -\frac{1}{4} \int d^5 x \left[W^{MNi} W_{MN}^i + r_V \{ \delta(y) + \delta(y - \pi R) \} W^{\mu\nu i} W_{\mu\nu}^i \right], \quad (9)$$

$$S_{scalar} = \int d^5 x \left[(D^M \Phi)^\dagger (D_M \Phi) + r_\phi \{ \delta(y) + \delta(y - \pi R) \} (D^\mu \Phi)^\dagger (D_\mu \Phi) \right], \quad (10)$$

$$S_{Yukawa} = - \int d^5 x \left[\lambda_t^5 \bar{\Psi}_L \tilde{\Phi} \Psi_R + r_y \{ \delta(y) + \delta(y - \pi R) \} \lambda_t^5 \bar{\phi}_L \tilde{\Phi} \chi_R + \text{h.c.} \right]. \quad (11)$$

$W_{MN}^i \equiv (\partial_M W_N^i - \partial_N W_M^i - g_2^5 f^{ijk} W_M^j W_N^k)$ represents the $SU(2)_L$ ($i = 1, 2, 3$) field strength tensor. Φ is the Higgs doublet and $\tilde{\Phi}$ satisfy the condition $\tilde{\Phi} \equiv i\sigma^2 \Phi^*$ with σ^2 being the Pauli matrix. r_V and r_ϕ are the coefficient of BLKT for gauge and scalar fields respectively while r_y represents the coefficient of boundary terms for Yukawa interactions. λ_t^5 denote the Yukawa interactions strength for the third generations in 5-D theory. Further, the 5-D gauge coupling g_2^5 is related to the 4-D coupling g_2 through,

$$g_2^5 = g_2 \sqrt{\pi R \left(1 + \frac{r_V}{\pi R} \right)}.$$

Appropriate KK-expansion of the fields which are involved in the above actions can be schematically written as:

$$W_\mu^i(x, y) = \sum_n W_\mu^{i(n)}(x) a^n(y); \quad W_4^i(x, y) = \sum_n W_4^{i(n)}(x) b^n(y), \quad (12)$$

and

$$\Phi(x, y) = \sum_n \Phi^{(n)}(x) h^n(y). \quad (13)$$

Note, that y -dependent profiles for the W^μ and W^4 must be different in the view of the fact that W^μ KK-tower must have a 0-mode, while the later shouldn't have such a mode in its KK-tower. In general, due to electroweak symmetry breaking, the eigenvalue equation for the gauge boson contains a term proportional to $(r_\phi - r_V)$ [26]. Consequently, KK-solutions of the gauge bosons are in general, different from Eq. 4. To avoid unnecessary complication we set $r_\phi = r_V$,

which we will keep in the rest of our analysis. Consequently, gauge boson KK-excitations have masses $m_{V^{(n)}} (= m_{\phi^{(n)}})$ which satisfy the same transcendental equations given in Eq. 8 with r_f replaced by $r_V (= r_\phi)$. Furthermore, this assumption helps us to fix the gauge properly in this non-trivial scenario. For a detail discussion of the W^μ and W^4 y -dependent profiles we refer to the ref. [26].

One must supplement the action for fermions and gauge bosons with the gauge-fixing action [26]:

$$S_{\text{gf}}^W = -\frac{1}{\xi_y} \int d^5x \left| \partial_\mu W^{\mu+} + \xi_y (\partial_y W^{4+} + iM_W \phi^+ \{1 + r_V (\delta(y) + \delta(y - \pi R))\}) \right|^2. \quad (14)$$

Here, W^{4+} is the 5th component of charged $SU(2)$ gauge boson, while ϕ^+ is the $T_3 = \frac{1}{2}$ component of the Higgs doublet. M_W is the 0-mode W -boson mass and ξ_y is connected with *physical* gauge fixing parameter ξ (with values 0 (Landau gauge), 1 (Feynman gauge) or ∞ (Unitary gauge)) via,

$$\xi = \xi_y \{1 + r_V (\delta(y) + \delta(y - \pi R))\}. \quad (15)$$

Using Eqs. 9, 10, and Eq. 14 we can write the bi-linear terms involving the KK-modes of $W^{4(n)\pm}$ and $\phi^{(n)\pm}$ in R_ξ gauge as:

$$\mathcal{L}_{W^{4(n)\pm}\phi^{(n)\pm}} = - \begin{pmatrix} W^{4(n)-} & \phi^{(n)-} \end{pmatrix} \begin{pmatrix} M_W^2 + \xi m_{V^{(n)}}^2 & -i(1 - \xi)M_W m_{V^{(n)}} \\ i(1 - \xi)M_W m_{V^{(n)}} & m_{V^{(n)}}^2 + \xi M_W^2 \end{pmatrix} \begin{pmatrix} W^{4(n)+} \\ \phi^{(n)+} \end{pmatrix}. \quad (16)$$

In addison to Goldstone bosons (with n^{th} mode mass square $\xi(M_W^2 + m_{V^{(n)}}^2)$):

$$G^{(n)\pm} = \frac{(m_{V^{(n)}} W^{4(n)\pm} \pm iM_W \phi^{(n)\pm})}{M_{W^{(n)}}},$$

we have additional physical charged Higgs pair (with n^{th} mode mass square $(M_W^2 + m_{V^{(n)}}^2)$):

$$H^{(n)\pm} = \frac{(m_{V^{(n)}} \phi^{(n)\pm} \pm iM_W W^{4(n)\pm})}{M_{W^{(n)}}}.$$

The fields $W^{\mu(n)\pm}$ and $H^{(n)\pm}$ have the same mass eigenvalue $M_{W^{(n)}} \equiv \sqrt{M_W^2 + m_{V^{(n)}}^2}$ and in 't-Hooft Feynman gauge ($\xi = 1$), $G^{(n)\pm}$ also correspond to the same mass eigenvalue.

Let us now examine the mixing of the quark sector. This mixing is only important for top quarks as it is driven by the Yukawa coupling. Using the modal expansions for fermions given in Eqs. 2 and 3 and substituting these in the actions given in Eq. 1 and Eq. 11 we can find the bi-linear terms involving the doublet and singlet states of the quarks. The mass matrix for n^{th} KK-level is as the following:

$$- \begin{pmatrix} \bar{\phi}_L^{(n)} & \bar{\phi}_R^{(n)} \end{pmatrix} \begin{pmatrix} m_{f^{(n)}} \delta^{nm} & m_t \mathcal{J}_1^{nm} \\ m_t \mathcal{J}_2^{mn} & -m_{f^{(n)}} \delta^{mn} \end{pmatrix} \begin{pmatrix} \chi_L^{(m)} \\ \chi_R^{(m)} \end{pmatrix} + \text{h.c.}, \quad (17)$$

where m_t is the top quark mass and $m_{f^{(n)}}$ are the solutions of transcendental equations given in Eq. 8. The overlap integrals (\mathcal{J}_1^{nm} and \mathcal{J}_2^{nm}) are of the form:

$$\mathcal{J}_1^{nm} = \left(\frac{1 + \frac{r_f}{\pi R}}{1 + \frac{r_y}{\pi R}} \right) \times \int_0^{\pi R} dy [1 + r_y \{\delta(y) + \delta(y - \pi R)\}] g_R^m f_L^n,$$

and

$$\mathcal{J}_2^{nm} = \left(\frac{1 + \frac{r_f}{\pi R}}{1 + \frac{r_y}{\pi R}} \right) \times \int_0^{\pi R} dy g_L^m f_R^n.$$

For both the cases of $n = m$ and $n \neq m$ the integral \mathcal{J}_1^{nm} is non zero. But for $r_y = r_f$, this integral equal to 1 (when $n = m$) or 0 ($n \neq m$). And the integral \mathcal{J}_2^{nm} is non zero only when $n = m$ and equal to 1 in the limit $r_y = r_f$. Using this equality (fermion and Yukawa BLT) condition we can easily avoid the mode mixing and construct simpler form of the fermion mixing matrix. In the rest of our analysis we will stick to the choice of equal r_y and r_f .

The resulting matrix (given in Eq. 17) can be diagonalised by following bi-unitary transformations for the left- and right-handed fields respectively:

$$U_L^{(n)} = \begin{pmatrix} \cos \alpha_{tn} & \sin \alpha_{tn} \\ -\sin \alpha_{tn} & \cos \alpha_{tn} \end{pmatrix}, \quad U_R^{(n)} = \begin{pmatrix} \cos \alpha_{tn} & \sin \alpha_{tn} \\ \sin \alpha_{tn} & -\cos \alpha_{tn} \end{pmatrix}, \quad (18)$$

where $\alpha_{tn} [= \frac{1}{2} \tan^{-1} \left(\frac{m_t}{m_{f^{(n)}}} \right)]$ is the mixing angle. The gauge eigen states $\Psi_L(x, y)$ and $\Psi_R(x, y)$ and mass eigen states T_t^1 and T_t^2 are related by the following relations:

$$\begin{aligned} \phi_L^{(n)} &= \cos \alpha_{tn} T_{tL}^{1(n)} - \sin \alpha_{tn} T_{tL}^{2(n)}, & \phi_R^{(n)} &= \sin \alpha_{tn} T_{tL}^{1(n)} + \cos \alpha_{tn} T_{tL}^{2(n)}, \\ \chi_L^{(n)} &= \cos \alpha_{tn} T_{tR}^{1(n)} + \sin \alpha_{tn} T_{tR}^{2(n)}, & \chi_R^{(n)} &= \sin \alpha_{tn} T_{tR}^{1(n)} - \cos \alpha_{tn} T_{tR}^{2(n)}. \end{aligned} \quad (19)$$

The eigen states are degenerate in mass, values of which are given by: $m_{T_t^1(n)} = m_{T_t^2(n)} = \sqrt{m_t^2 + m_{f^{(n)}}^2} \equiv M_{t^{(n)}}$.

Feynman rules (in 't-Hooft Feynman gauge) which follow from the above action and necessary for our calculation are listed in Appendix C. One can see that some of the interactions listed in Appendix C have been modified with respect to their UED counterparts by some overlap integrals. These overlap integrals are generated while arriving at the 4-D effective action from 5-D one by inserting the appropriate y -dependent profiles in the (5-D) action and integrating over the y -direction. Here we present the overlap integrals which will frequently occur in our calculation.

- Interaction of a 0-mode fermion with a KK-fermion (n^{th} mode) and a KK-gauge boson (m^{th} mode):

$$I_V^{nm} = \sqrt{\pi R \left(1 + \frac{r_V}{\pi R}\right)} \times \begin{cases} \int_0^{\pi R} dy [1 + r_f \{\delta(y) + \delta(y - \pi R)\}] a^m f_L^n f_L^0, \\ \int_0^{\pi R} dy [1 + r_f \{\delta(y) + \delta(y - \pi R)\}] a^m g_R^n g_R^0. \end{cases} \quad (20)$$

- Interaction of a 0-mode fermion with a KK-fermion (n^{th} mode) and the m^{th} KK-mode of 5^{th} component of a gauge boson:

$$I_V^{nm} = \sqrt{\pi R \left(1 + \frac{r_V}{\pi R}\right)} \times \begin{cases} \int_0^{\pi R} dy b^m g_L^n f_L^0, \\ \int_0^{\pi R} dy b^m f_R^n g_R^0. \end{cases} \quad (21)$$

In Eq. 20 a^m is the wave function (m^{th} KK-mode) for gauge field, with Lorentz index μ . While in Eq. 21 b^m is the wave function (m^{th} KK-mode) for 5^{th} component of the corresponding gauge field.

- Yukawa interactions of fermions and scalars:

$$I_Y^{nm} = \sqrt{\pi R \left(1 + \frac{r_V}{\pi R}\right)} \times \begin{cases} \int_0^{\pi R} dy [1 + r_f \{\delta(y) + \delta(y - \pi R)\}] h^m f_L^n g_R^0, \\ \int_0^{\pi R} dy [1 + r_f \{\delta(y) + \delta(y - \pi R)\}] h^m g_R^n f_L^0. \end{cases} \quad (22)$$

In the above, h^m is the wave function (m^{th} KK-mode) for scalar field.

Now for, $r_\phi = r_V$ we have $a^m \equiv h^m$ and for $r_f = r_y$, $I_V^{nm} \equiv I_Y^{nm}$, for $n = m$ let us call it I_1^n , and is given by:

$$I_1^n = 2 \sqrt{\frac{1 + \frac{r_V}{\pi R}}{1 + \frac{r_f}{\pi R}}} \left[\frac{1}{\sqrt{1 + \frac{r_f^2 m_{f(n)}^2}{4} + \frac{r_f}{\pi R}}} \right] \left[\frac{1}{\sqrt{1 + \frac{r_V^2 m_{V(n)}^2}{4} + \frac{r_V}{\pi R}}} \right] \frac{m_{V(n)}^2}{(m_{V(n)}^2 - m_{f(n)}^2)} \frac{(r_f - r_V)}{\pi R}, \quad (23)$$

and we denote $I_V^{nm} = I_2^{nm}$. Let us call it I_2^n for $n = m$ and is given by:

$$I_2^n = 2 \sqrt{\frac{1 + \frac{r_V}{\pi R}}{1 + \frac{r_f}{\pi R}}} \left[\frac{1}{\sqrt{1 + \frac{r_f^2 m_{f(n)}^2}{4} + \frac{r_f}{\pi R}}} \right] \left[\frac{1}{\sqrt{1 + \frac{r_V^2 m_{V(n)}^2}{4} + \frac{r_V}{\pi R}}} \right] \frac{m_{V(n)} m_{f(n)}}{(m_{V(n)}^2 - m_{f(n)}^2)} \frac{(r_f - r_V)}{\pi R}. \quad (24)$$

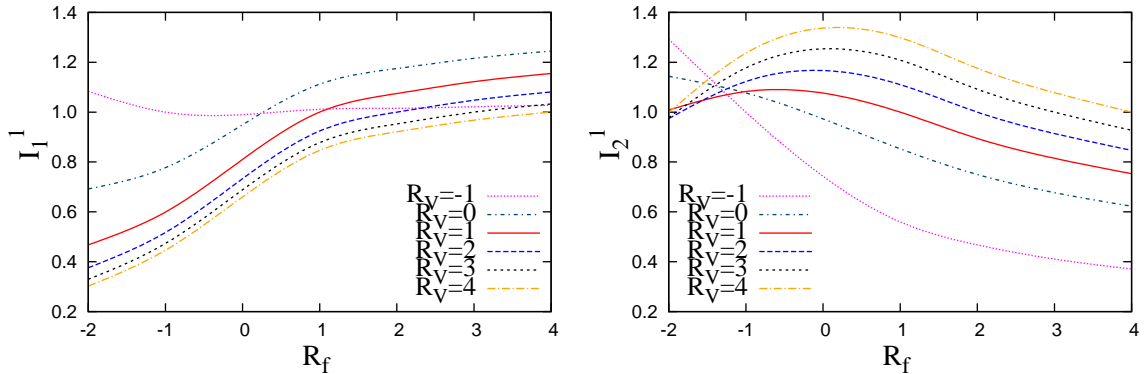


Figure 1: Variation of the overlap integrals I_1^1 (left panel) and I_2^1 (right panel) defined in Eqs. 23 and 24 with R_f for six different values of R_V .

These two overlap integrals play a crucial role in our analysis. Many of the couplings used in the following calculation are hallmarked by the presence these integrals which can be explicitly seen in the Feynman rules listed in Appendix C. First of all, in the limit $r_f = r_V$, both of these overlap integrals become unity, setting all the nmUED couplings equal to their UED values. For the purpose of illustration, variations of the integrals I_1^1 and I_2^1 ($n = m = 1$) with $r_f/R(= R_f)$ and $r_V/R(= R_V)$ have been presented in Fig. 1. Left (right) panel shows the variation of I_1^1 (I_2^1) with R_f for six different values of R_V . We have presented these integrals for both positive as well as negative values of R_V and R_f . Let us first discuss the pattern of these integrals for positive values of R_V . In this case, while I_1^1 increases with R_f , I_2^1 initially increases before it starts decreasing with R_f . On the other hand if R_V is negative, I_1^1 is almost independent of R_f , but I_2^1 steadily decreases with R_f over the entire range of its values used in Fig. 1. At this point we would like to make some comments which could help the reader to understand the nature of the plots. The first two factors (one under the square root sign and the other in the first square bracket involving r_f only) decreases with R_f in both of these integrals. Among the remaining factors, term proportional to $m_{V(1)}^2$ (in I_1^1) slowly diminish in magnitude with R_f . The remaining factor proportional to $(R_f - R_V)$ increases with R_f . When R_V is negative ($= -1$), due to an interplay between the term proportional to $m_{V(1)}^2$ and remaining factors, I_1^1 remains almost independent with R_f . This explains the qualitative departure of the overlap integral I_1^1 for negative and positive values of R_V . Furthermore, as $m_{f(1)}$ is a decreasing function of R_f , in I_2^1 the presence of a factor proportional to $m_{V(1)}m_{f(1)}$ (instead of $m_{V(1)}^2$ in I_1^1) offers additional damping to the magnitude of I_2^1 . And apart from some lower values of R_f , I_2^1 always decreases with R_f .

Before going into the main calculation, let us comment on the range of values of BLT parameters used in our analysis. In general BLT parameters can positive or negative. A careful look into the Eq. 7 would reveal that, for $r_f/R = -\pi$ the 0-mode solution becomes divergent. And beyond $r_f/R = -\pi$ the 0-mode fields become ghost-like. Any other values of BLT parameters greater than $-\pi$ are acceptable. However, as BLT parameters change from positive to negative domain, corresponding KK-masses would increase thus diminishing the values of loop functions described below. This in turn decrease the magnitudes of the branching ratios of our interest.

III $B_{s(d)} \rightarrow \mu^+ \mu^-$ in nmUED

Stage has now been set to discuss the subject of our attention, namely the branching ratio of $B_{s(d)}$ into $\mu^+ \mu^-$ pair. The effective Hamiltonian for $B_{s(d)} \rightarrow \mu^+ \mu^-$ decay is given by:

$$\mathcal{H}_{\text{eff}} = -\frac{G_F}{\sqrt{2}} \frac{\alpha}{2\pi \sin^2 \theta_w} V_{tb}^* V_{ts(d)} \eta_Y Y(x_t, r_f, r_V, R^{-1}) [\bar{b} \gamma_\mu (1 - \gamma_5) s(d)] [\bar{\mu} \gamma^\mu (1 - \gamma_5) \mu] + \text{h.c.}, \quad (25)$$

where G_F is the Fermi constant, V_{ij} are the Cabibbo-Kobayashi-Maskawa (CKM) matrix elements, α is the fine structure constant, η_Y is the QCD factor and θ_w is the Weinberg angle. The function $Y(x_t, r_f, r_V, R^{-1})$ is the total contributions coming from Z -penguins, self-energy and box diagrams:

$$Y(x_t, r_f, r_V, R^{-1}) = C(x_t, r_f, r_V, R^{-1}) + B(x_t, r_f, r_V, R^{-1}), \quad (26)$$

where $C(x_t, r_f, r_V, R^{-1})$ originates from penguins and self energy diagrams (Fig. 2 and Fig. 3 respectively) and is defined as:

$$C(x_t, r_f, r_V, R^{-1}) = C_0(x_t) + \sum_{n=1}^{\infty} C_n(x_{t(n)}, x_{u(n)}). \quad (27)$$

Here, $C_0(x_t)$ is the SM contribution:

$$C_0(x_t) = \frac{x_t}{8} \left[\frac{x_t - 6}{x_t - 1} + \frac{3x_t + 2}{(x_t - 1)^2} \ln x_t \right], \quad (28)$$

while the second term represents the total KK-contribution that is being calculated from the Z -penguin diagrams and self-energy diagrams (Figs. 2 and 3) originating from the nmUED framework. The function $C_n(x_{t(n)}, x_{u(n)})$ is defined as:

$$C_n(x_{t(n)}, x_{u(n)}) = F(x_{t(n)}) - F(x_{u(n)}), \quad (29)$$

where $F(x_{t(n)})$ and $F(x_{u(n)})$ arises respectively, from the contributions of the $T_t^{1(n)}$, $T_t^{2(n)}$ and $T_u^{1(n)}$, $T_u^{2(n)}$ modes. The function $F(x_{t(n)})$ takes the form:

$$F(x_{t(n)}) = \sum_{i=1}^8 F_i(x_{t(n)}) + \left(\frac{1}{2} - \frac{1}{3} \sin^2 \theta_w \right) \sum_{i=1}^2 \Delta S_i(x_{t(n)}). \quad (30)$$

Moreover F_i denote the contributions those are coming from Z -penguin diagrams (1-8 in Fig. 2) and ΔS_i represent the contributions of self-energy diagrams (Ia-IIb in Fig. 3) which are necessary for calculation of the electroweak counter terms. While the function $F(x_{u(n)})$ is given by:

$$F(x_{u(n)}) = F(x_{t(n)}) \Big|_{x_t \rightarrow 0}. \quad (31)$$

$F(x_{u(n)})$ are subtracted in the above (Eq. 29) to take into account of the contributions of KK-excitation of first two generations of quarks in Z -penguins and self-energy diagrams, exploiting the GIM-mechanism. $F(x_{t(n)})$ in nmUED framework is given by the following expression which is drastically different from that of UED due to the presence of integrals I_1^n and I_2^n :

$$\begin{aligned}
F(x_{t(n)}) = & \left[\frac{1}{8} \left\{ -\ln M_{t(n)}^2 - \frac{3}{2} + h_q(x_{t(n)}) \right\} - \frac{1}{4} x_{t(n)} h_q(x_{t(n)}) \frac{m_{f(n)}^2}{M_{t(n)}^2} \right] (I_1^n)^2 \\
& - \frac{3}{4} \left[-\ln M_{W(n)}^2 - \frac{1}{6} - x_{t(n)} h_w(x_{t(n)}) \right] (I_1^n)^2 - \frac{1}{2} h_w(x_{t(n)}) \frac{m_{f(n)}^2}{M_{W(n)}^2} (I_1^n)^2 \\
& + \left[\frac{1}{16} \left\{ -\ln M_{t(n)}^2 - \frac{1}{2} + h_q(x_{t(n)}) \right\} (I_2^n)^2 - \frac{1}{8} x_{t(n)} h_q(x_{t(n)}) \left\{ \frac{m_{f(n)}^4}{M_{t(n)}^2 m_{V(n)}^2} + \frac{m_t^4}{M_{t(n)}^2 M_W^2} \right\} (I_1^n)^2 \right] \\
& - \frac{1}{16} [2(I_2^n)^2 + x_t(I_1^n)^2] \left[-\ln M_{W(n)}^2 + \frac{1}{2} - x_{t(n)} h_w(x_{t(n)}) \right] \\
& + \frac{1}{8} \left[-\frac{1}{2} \left\{ \frac{1+x_{t(n)}}{1-x_{t(n)}} + \frac{2x_{t(n)}^2 \ln x_{t(n)}}{(1-x_{t(n)})^2} \right\} - \ln M_{W(n)}^2 \right] (I_1^n)^2 \\
& + \frac{1}{16} [(I_2^n)^2 + x_t(I_1^n)^2] \left[\frac{1}{2} \left\{ \frac{1-3x_{t(n)}}{1-x_{t(n)}} - \frac{2x_{t(n)}^2 \ln x_{t(n)}}{(1-x_{t(n)})^2} \right\} - \ln M_{W(n)}^2 \right]. \tag{32}
\end{aligned}$$

Expressions for h_q and h_w are listed in Appendix A (Eqs. A-9 and A-10).

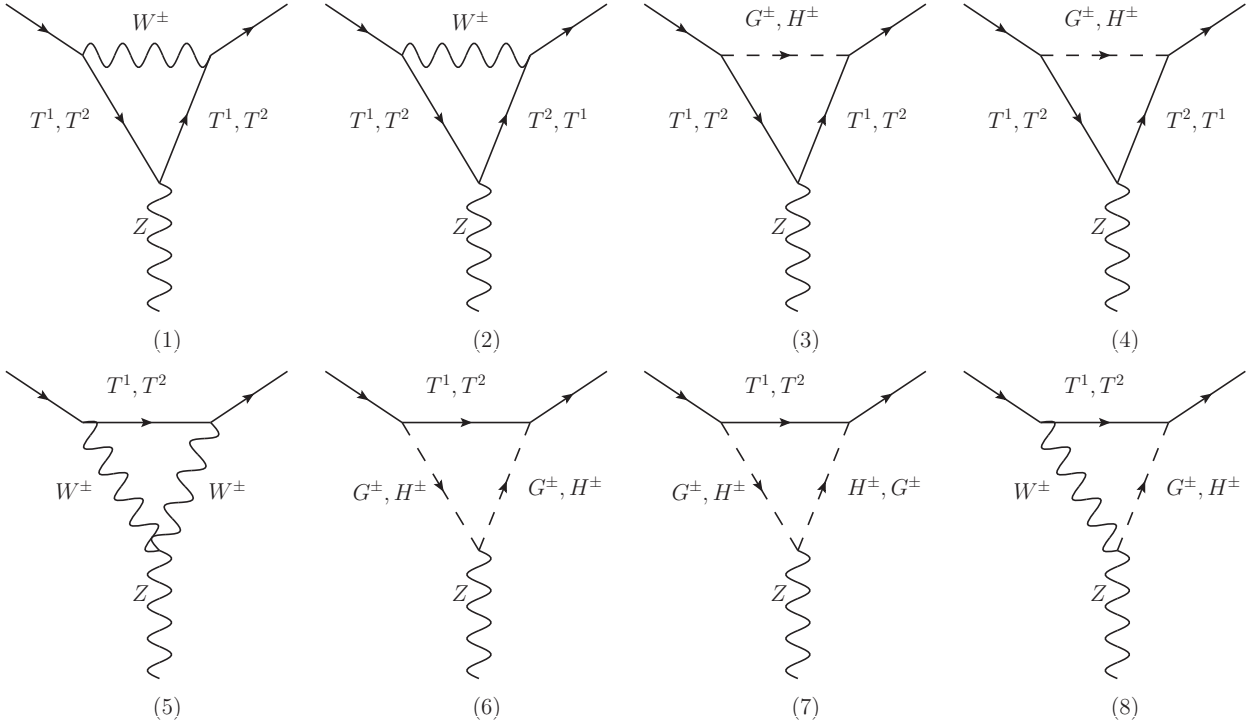


Figure 2: Z -penguin diagrams contributing to the decay of $B_{s(d)}$.

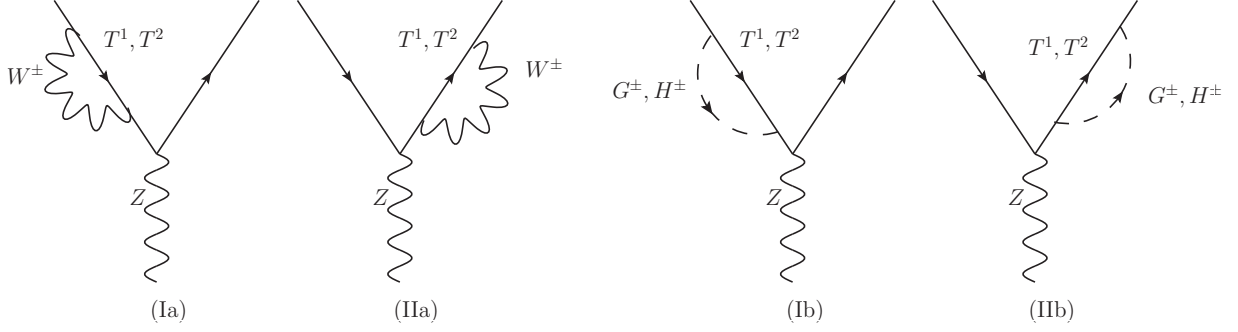


Figure 3: Self-energy diagrams contributing to the decay of $B_{s(d)}$.

$B(x_t, r_f, r_V, R^{-1})$ in Eq. 26 is given by:

$$B(x_t, r_f, r_V, R^{-1}) = -B_0(x_t) + \sum_{n=1}^{\infty} B_n(x_{t(n)}, x_{u(n)}, x_{\nu(n)}). \quad (33)$$

$B_0(x_t)$ again represents the SM contribution to the box diagrams:

$$B_0(x_t) = \frac{1}{4} \left[\frac{x_t}{1-x_t} + \frac{x_t}{(x_t-1)^2} \ln x_t \right], \quad (34)$$

and the second term denotes the total KK-contribution that is evaluated from the box diagrams (Fig. 4). $B_n(x_{t(n)}, x_{u(n)}, x_{\nu(n)})$ is defined as:

$$B_n(x_{t(n)}, x_{u(n)}, x_{\nu(n)}) = H(x_{t(n)}, x_{\nu(n)}) - H(x_{u(n)}, x_{\nu(n)}). \quad (35)$$

In nmUED framework, expression for $H(x_{t(n)}, x_{\nu(n)})$ is given as the following:

$$\begin{aligned} H(x_{t(n)}, x_{\nu(n)}) = (I_1^n)^4 & \left[-\frac{1}{4} \frac{M_W^2}{M_{W(n)}^2} U(x_{t(n)}, x_{\nu(n)}) + \frac{1}{2} \frac{M_W^2 M_{t(n)}^2 m_{f(n)}^2}{M_{W(n)}^6} \tilde{U}(x_{t(n)}, x_{\nu(n)}) \right. \\ & + \frac{1}{2} \frac{M_W^2 m_{f(n)}^2}{M_{W(n)}^6} \left(\frac{M_W^2 m_{f(n)}^2}{m_{V(n)}^2} - m_t^2 \right) \tilde{U}(x_{t(n)}, x_{\nu(n)}) - \frac{1}{8} \frac{M_W^2 m_{f(n)}^2}{M_{W(n)}^6} \left(\frac{M_W^2 m_{f(n)}^2}{m_{V(n)}^2} - m_t^2 \right) U(x_{t(n)}, x_{\nu(n)}) \\ & \left. - \frac{1}{16} \frac{M_W^2 M_{t(n)}^2 m_{f(n)}^2}{M_{W(n)}^6} U(x_{t(n)}, x_{\nu(n)}) - \frac{1}{16} \frac{M_W^2}{M_{W(n)}^6} \left(\frac{M_W^4 m_{f(n)}^4}{m_{V(n)}^4} + m_t^2 m_{f(n)}^2 \right) U(x_{t(n)}, x_{\nu(n)}) \right], \quad (36) \end{aligned}$$

and $H(x_{u(n)}, x_{\nu(n)})$ is defined through:

$$H(x_{u(n)}, x_{\nu(n)}) = H(x_{t(n)}, x_{\nu(n)}) \Big|_{x_t \rightarrow 0}. \quad (37)$$

The expressions for the functions U and \tilde{U} can be found in Appendix B (Eqs. B-7 and B-8).

The definition of B_n (given in Eq. 35) are again in order to take into account the contributions from KK-excitations of first two generations of quarks into the calculation.

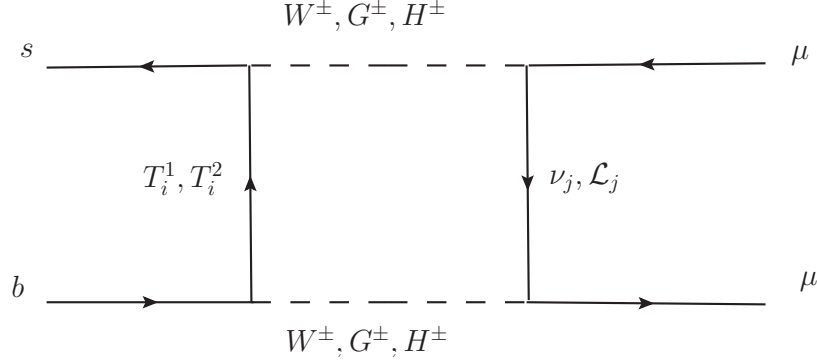


Figure 4: Box diagrams contributing to the decay of $B_{s(d)}$.

Note that $x_t = \frac{m_t^2}{M_W^2}$, and $x_{t(n)} = \frac{M_{t(n)}^2}{M_{W(n)}^2} = \frac{m_t^2 + m_{f(n)}^2}{M_W^2 + m_{V(n)}^2}$, $m_{f(n)}$ and $m_{V(n)}$ are the solutions of Eq. 8 corresponding to the BLKT parameters r_f and r_V respectively.

Finally one can express the branching ratio of $B_{s(d)} \rightarrow \mu^+ \mu^-$ in terms of Y and other parameters as:

$$\begin{aligned}
 Br(B_{s(d)} \rightarrow \mu^+ \mu^-) &= \tau(B_{s(d)}) \frac{G_F^2}{\pi} \left(\frac{\alpha}{4\pi \sin^2 \theta_w} \right)^2 F_{B_{s(d)}}^2 m_\mu^2 m_{B_{s(d)}} \\
 &\quad \sqrt{1 - 4 \frac{m_\mu^2}{m_{B_{s(d)}}^2} |V_{tb}^* V_{ts(d)}|^2} Y^2(x_t, r_f, r_V, R^{-1}),
 \end{aligned} \tag{38}$$

where, $F_{B_{s(d)}}$ is the $B_{s(d)}$ meson decay constant and $\tau(B_{s(d)})$ is the life time. m_μ and $m_{B_{s(d)}}$ are the masses of muon and $B_{s(d)}$ meson respectively.

We would like to point out that the total contribution from UED is obtained by summing C_n s and B_n s over KK-modes (starting from $n = 1$). It can be checked easily that these quantities tend to vanish when $R^{-1} \rightarrow \infty$, showing the decoupling nature of the new physics in this case. While estimating the contribution from the KK-excitation, in the one loop mediated amplitudes, we have used only those interactions which couples a 0-mode field to pair of KK-excitations with same KK-number. However, in a manifestly KK-parity conserving theory, there can be non zero interactions among a 0-mode field with two different KK-excitations, say, with unequal KK-number n and m , modulo $n + m$ is an even integer. We have explicitly checked that $0 - n - m$ interactions are suppressed with respect to the $0 - n - n$ interactions [18] and we neglect those while estimating the $B_{s(d)} \rightarrow \mu^+ \mu^-$ interactions.

In our calculation, we have neglected the masses of the external quarks and while evaluating the Z -penguins and box diagrams, momenta of the external legs have been assumed to be vanishing.

IV Results

We are now equipped to present our results. Before we proceed further let us present the experimentally measured value [27] of $Br(B_{s(d)} \rightarrow \mu^+\mu^-)$ along with the SM prediction [24, 27] for the same in Table 1. Central values of experimentally measured branching ratios of B_s (B_d) are nearly one (two)-standard deviation away from its SM prediction.

Branching ratio	SM prediction	Experimental value
$B_s \rightarrow \mu^+\mu^-$	$(3.66 \pm 0.23) \times 10^{-9}$	$(2.8_{-0.6}^{+0.7}) \times 10^{-9}$
$B_d \rightarrow \mu^+\mu^-$	$(1.06 \pm 0.09) \times 10^{-10}$	$(3.9_{-1.4}^{+1.6}) \times 10^{-10}$

Table 1: SM prediction for $B_{s(d)} \rightarrow \mu^+\mu^-$ branching ratios and their experimental measured values.

We will now discuss the method, that has been used in the following, for the numerical estimation of $Br(B_s \rightarrow \mu^+\mu^-)$. We will follow similar procedure for the estimation of $Br(B_d \rightarrow \mu^+\mu^-)$. Numerical value of the B_s branching ratio, quoted in Table 1 includes higher order corrections (NNLO-QCD and NLO-EW corrections [24]) to the branching ratio in the framework of the SM. The total decay amplitude in the UED framework is a sum of contributions from different KK-levels (including the contribution from 0-level which is nothing but the SM). We expect that higher order corrections to the decay amplitude originating from higher KK-modes would be in the same ballpark that of the SM (0-mode). So to (approximately) take into account the effects of higher order corrections into our result we have estimated $Br(B_s \rightarrow \mu^+\mu^-)$ in UED as,³

$$Br(B_s \rightarrow \mu^+\mu^-)_{UED} = Br(B_s \rightarrow \mu^+\mu^-)_{SM} \left(\frac{Y}{Y_0} \right)^2. \quad (39)$$

Here, Y total contribution (originating from 0 and higher KK-modes) defined in Eq. 26, while $Y_0(\equiv C_0 + B_0)$ is only the 0-mode (SM) contribution. Expressions for C_0 and B_0 are given in Eq. 28 and Eq. 34 respectively. For numerical estimation of the above branching ratio, we have used the central value (3.66×10^{-9}) for $Br(B_s \rightarrow \mu^+\mu^-)_{SM}$, following the ref. [27].

In the above, we have expressed $Br(B_s \rightarrow \mu^+\mu^-)_{UED}$ in terms of $Br(B_s \rightarrow \mu^+\mu^-)_{SM}$. Consequently, the relevant input parameters for numerical evaluation of the above branching ratio

³This method is somehow similar to find a k -factor (the ratio of branching ratios with higher order correction and without any correction in our case) in the SM and then multiply the leading order branching ratio in UED by this k -factor. In absence of a full higher order correction in UED framework, this approximation is not very bad, as the higher KK-modes of t -quark and W -bosons, running in the triangle or box diagrams, have similar couplings to the SM particles in the initial and the final state.

are top-quark and W -boson masses respectively, which are necessary for evaluation of the functions Y_0 and Y . We use the values of these parameters following the ref. [28]. Values of these parameters used in ref. [24] are same as the values in ref. [28]⁴.

Any contribution to the $B_{s(d)} \rightarrow \mu^+ \mu^-$ branching ratio from the SM and beyond the SM goes into the function Y as defined in Eq. 38. The dominant contribution to Y comes from the diagrams (3), (4), (6) and (7) of Fig. 2 (Z -penguins); (Ib) and (IIb) of Fig. 3 (self-energies). These amplitudes are proportional to $g_2 \lambda_t^2$, where λ_t being the top-Yukawa coupling. Box diagram contributions are not significant in comparison to the penguins⁵. One must perform a sum over the KK-modes while evaluating the C and B -functions, which contribute to Y . In view of a recent analysis correlating the SM Higgs mass and cut-off scale of UED model [29], we restrict ourselves upto 5 KK-levels. Previous practice was to use 20-30 KK-levels while summing up the contributions from KK-modes. However, we have explicitly checked that numerical results would not change to a significant level as the sum over the KK-modes, in this case is converging⁶. At the end of following sub-section, we will present a table comparing the B_s branching ratios calculated with 5 KK-levels vis-a-vis 20 KK-levels in support of our assumption.

The main results of our analysis *i.e.* variation of the branching ratio ($B_s \rightarrow \mu^+ \mu^-$) with R^{-1} for several values of R_f are presented in Fig. 6. Same have been presented for B_d in Fig. 7. Six different panels show the dependence of branching ratios with R_V . We will be discussing the implications of these results in the framework of nmUED. But before delving into that, we would like to discuss the consequences of the result in the framework of UED itself.

IV.1 Reviewing the limits on R^{-1} in UED framework

To start with we will focus on the $B_{s(d)}$ meson branching ratio to $\mu^+ \mu^-$ in the UED frame work. The expression for F^n and H^n defined in Eqs. 32 and 36 would result into their UED forms once we set $r_V = r_f = 0$. In this limit the overlap integrals I_1^n and I_2^n become unity and the masses of the KK-excitations in n^{th} KK-mode become equal to nR^{-1} . We check that our expressions of C and B in this limit agree exactly with the one in ref. [25]⁷. In Fig. 5 we have plotted the $B_{s(d)} \rightarrow \mu^+ \mu^-$ branching ratio with R^{-1} in UED framework (black dashed curve in each panel). Steady decrement of the branching ratio with increasing R^{-1} is an artefact of increasing KK-masses with R^{-1} . This line intersects the horizontal line (light shaded) (4.2×10^{-9} for B_s and 7.1×10^{-10} for B_d) which correspond to the 95% C.L. upper limit on the experimentally measured branching ratio of B_s (left panel of Fig. 5) and B_d (right panel of Fig. 5). Thus the

⁴We have used $M_W = 80.38$ GeV and $m_t = 173.21$ GeV.

⁵As for example, in nmUED model, for $R^{-1} = 1$ TeV, $R_f = R_V = 1$ after summing over 5 KK-levels $C = 0.9116$ while $B = 0.1856$. For $R^{-1} = 2$ TeV, $R_f = R_V = 1$, $C = 0.8915$ while $B = 0.1846$. The smallness of the box diagram contribution in comparison to the penguins, has also been pointed out in ref. [25]

⁶It has been shown in [30], the KK-sum in case of one loop calculation (like the one in the present case) in UED with one extra space like dimension is always converging.

⁷The authors of ref. [25] have not considered any radiative corrections to the KK-masses, consequently mass of a n^{th} KK-excitation is nR^{-1} in their analysis.

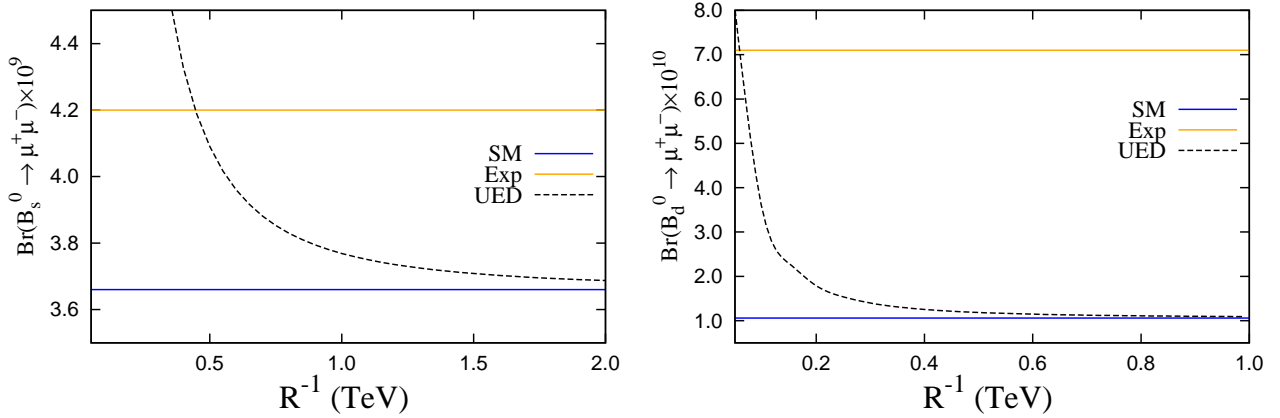


Figure 5: Left (right) panel: Variation of the branching ratio ($B_s(B_d) \rightarrow \mu^+ \mu^-$) with R^{-1} in UED model. The black dashed line in each panel represents the UED curve (corresponds to $r_V/R = R_V = 0$ and $r_f/R = R_f = 0$ case). The dark shaded horizontal line represents the SM prediction for the above branching ratio, while the light shaded horizontal line represents the 95 % C.L. upper limit on the experimentally measured $B_{s(d)}$ branching ratio to muon pair.

R^{-1} values corresponding to these intersections would give rise to a 95% C.L. lower limit on the value of R^{-1} . One can see this limit from B_s decay comes out to be 454 GeV. While deriving this limit, we have neglected the theoretical error on $Br(B_s \rightarrow \mu^+ \mu^-)$. One can easily see from Table 1, that theoretical error on the SM estimate of this branching ratio is around 6% and we expect that theory error in the UED framework will be of the same order. And this is small compared to the experimental error (nearly 25 %) on the measured value of the branching ratio. Our results presented in Fig. 5, thus correspond to a vanishing theoretical error on the B_s branching ratio.

The lower bound on R^{-1} which results from B_d decay ($R^{-1} \sim 60$ GeV) is not so promising. To put our observation into the proper context we would briefly mention the bounds on R^{-1} that result from other processes. Consideration of $(g - 2)_\mu$ [31], ρ -parameter [32], FCNC process [25, 33, 34] and electroweak observables like R_b [18, 35] would result into a lower limit on R^{-1} which is in the ballpark of 300 GeV. Consideration of radiative B -meson decay puts a lower limit of 600 GeV on R^{-1} [36]. While the projected lower limit on R^{-1} using tri-lepton signal at 8 TeV LHC is 1.2 TeV [37].

IV.2 Bounds from the nmUED

We are now in a position to discuss our results in the context of nmUED. Numerical results from the calculation presented in the previous section are presented in Figs. 6 and 7 for B_s and B_d meson branching ratios to muon pair respectively. In each of the figures six different panels represents the results for six different choices for gauge BLKT, R_V . While in each panel

different line represents the variation of the branching ratio with R^{-1} with different values of fermion BLKT coefficients, R_f .

The monotonic decreasing nature of the branching ratio with increasing R^{-1} is the same as in UED and has been explained in the above. The dependence on the other parameters could be easily understood as the following. For a given R^{-1} , masses of KK-excitations of fermions, gauge bosons and scalars decrease with increasing R_f and R_V . This in turn, increase the decay width of B_s and B_d to $\mu^+\mu^-$. Apart from KK-masses the other determining factors in our calculation are the overlap integrals defined in Eqs. 23 and 24. We have already noted their dependencies on R_f and R_V .

One can see that $B_s \rightarrow \mu^+\mu^-$ branching ratio increases with the increment of both of these BLKT coefficients. Dependence on R_V is mild while it is more sensitive to any change of R_f . This can be understood again by looking at the interactions used in this calculation listed in Appendix C. A careful look at the Feynman rules reveals that I_1^n and I_2^n modify the interactions of 3^{rd} generations of quarks with charged-Higgs scalar and 5^{th} component of W -boson respectively. The first one being top-Yukawa, is dominant over the second one, which is $SU(2)$ gauge interaction. Thus I_1^n which appears with top-Yukawa, has a better control on the $B_s \rightarrow \mu^+\mu^-$ amplitude, which increases both with R_f and R_V . Dependence of $Br(B_d \rightarrow \mu^+\mu^-)$ on R^{-1} and BLKT parameters can be explained in the same way. The decay of B_d to $\mu^+\mu^-$ is suppressed with respect to the B_s by a factor of $\left(\frac{V_{td}}{V_{ts}}\right)^2$. Finally we would like to add that for negative values of BLKT parameters, above branching ratio is always less than the value for the same in the UED model. This could be easily accounted by the suppression of decay amplitude due to heavier (than in the UED case) KK-excitation in nmUED framework for negative values of BLKT parameters.

Finally in Fig. 8 (right panel), the exclusion region in $R_f - R^{-1}$ plane, has been presented for six different choices of R_V . The region under a particular line (corresponding to a fixed value of R_V) has been excluded at 95% C.L. by comparing the experimentally measured $Br(B_s \rightarrow \mu^+\mu^-)$ to its theoretical prediction in the framework of nmUED. This plot is a summary of the results presented in Fig. 6. The lines represent the contours of constant branching ratios of $B_s \rightarrow \mu^+\mu^-$ corresponding to the 95% C.L. upper limit (4.2×10^{-9}) of its experimentally determined value. Features of this contours can be easily understood in the light of our discussion above. Higher values of R^{-1} would increase the KK-masses hence pulling down the decay width (and branching ratio). To compensate this one must increase R_f and R_V , which control the decay dynamics in two ways. First of all, these would pull down the masses and R_f would also increase the couplings through the overlap integral I_1^n . While an increasing R_V would decrease I_1^n but increase I_2^n . Overall, with increasing R_V , decay width mildly increase in contrast to R_f , which would increase the decay width more sharply with its increment.

We would like to show the difference in the derived lower limits on R^{-1} due to taking into account 5 KK-levels vis-a-vis 20 KK-level while performing the KK-level summation. One can see from Table 2, that the lower limits on R^{-1} (in TeV) derived from our analysis is not very much sensitive to the number of KK-level used in the summation.

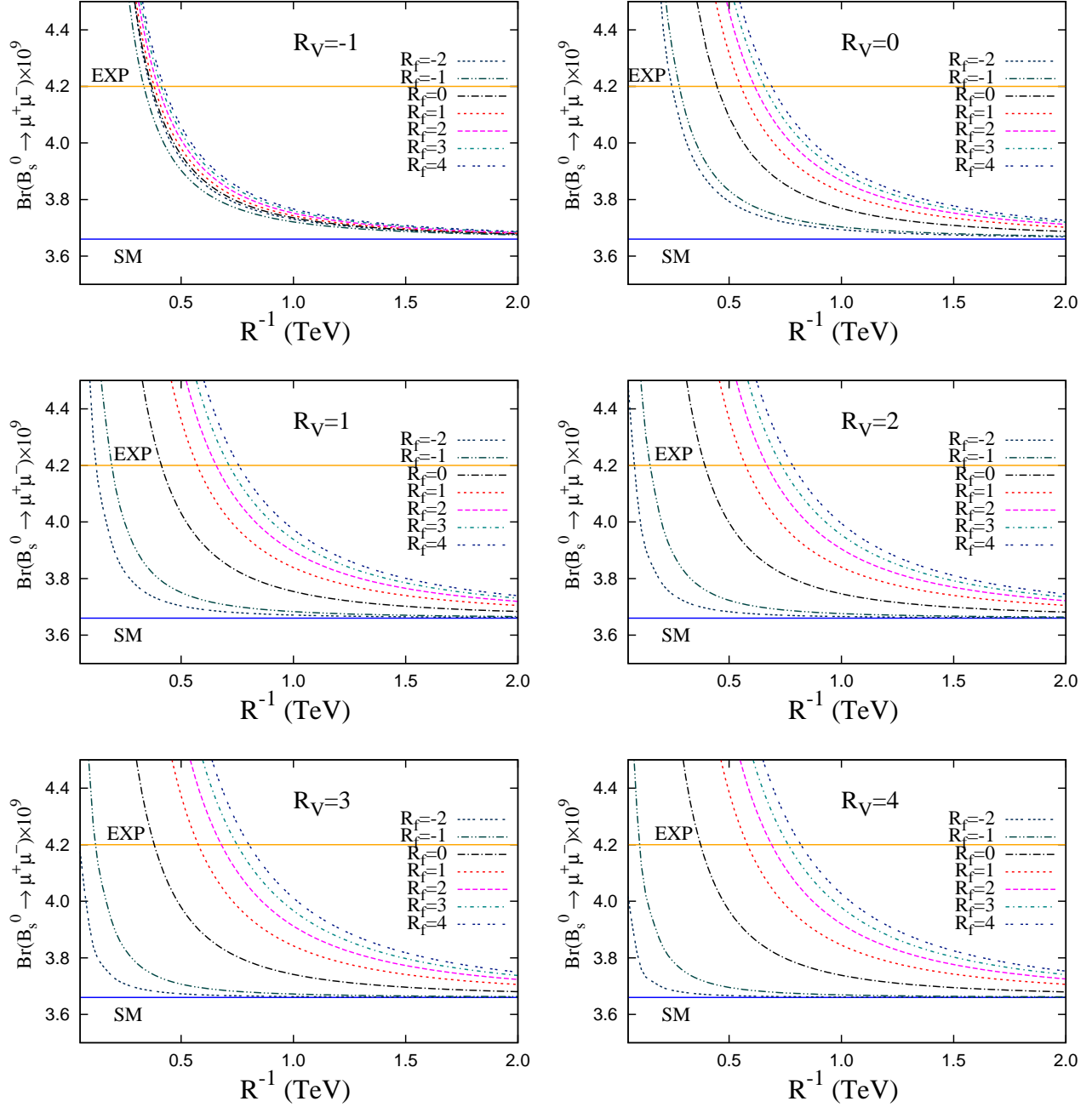


Figure 6: Variation of the branching ratio ($B_s \rightarrow \mu^+\mu^-$) with R^{-1} for several values of $R_f = r_f/R$. The six panels correspond to different $R_V = r_v/R$. The dark shaded horizontal line represents the SM prediction for the above branching ratio, while the light shaded horizontal line represents the 95 % C.L. upper limit on the experimentally measured B_s branching ratio to muon pair.

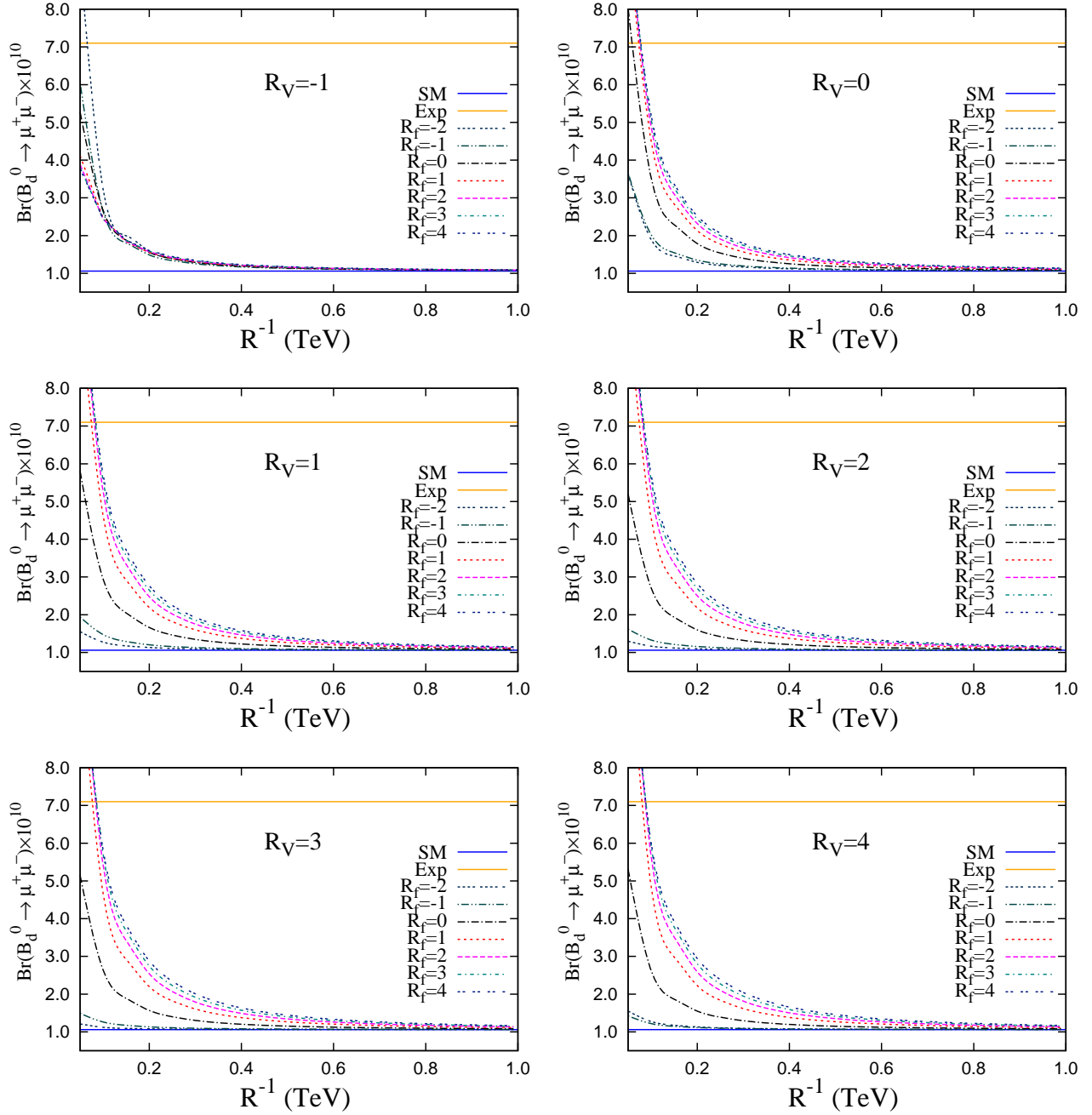


Figure 7: Variation of the branching ratio ($B_d \rightarrow \mu^+ \mu^-$) with R^{-1} for several values of $R_f = r_f/R$. The six panels correspond to different $R_V = r_V/R$. The dark shaded horizontal line represents the SM prediction for the above branching ratio, while the light shaded horizontal line represents the 95 % C.L. upper limit on the experimentally measured B_d branching ratio to muon pair.

R_f	$R_V = -1$		$R_V = 0$		$R_V = 1$		$R_V = 2$		$R_V = 3$		$R_V = 4$	
	5 KK-level	20 KK-level	5 KK-level	20 KK-level	5 KK-level	20 KK-level	5 KK-level	20 KK-level	5 KK-level	20 KK-level	5 KK-level	20 KK-level
-2	0.333	0.357	0.246	0.260	0.119	0.122	0.077	0.081	0.045	0.050	0.035	0.039
-1	0.361	0.378	0.280	0.300	0.191	0.192	0.146	0.150	0.119	0.120	0.101	0.105
0	0.368	0.380	0.454	0.460	0.412	0.418	0.392	0.402	0.383	0.392	0.373	0.384
1	0.381	0.399	0.553	0.567	0.586	0.603	0.588	0.610	0.590	0.617	0.593	0.621
2	0.399	0.406	0.617	0.624	0.672	0.686	0.682	0.700	0.693	0.717	0.698	0.723
3	0.403	0.409	0.661	0.664	0.734	0.745	0.752	0.765	0.766	0.786	0.770	0.792
4	0.410	0.416	0.694	0.701	0.780	0.783	0.800	0.810	0.820	0.834	0.825	0.838

Table 2: Lower limits on R^{-1} (in TeV) derived from B_s decay branching ratio to $\mu^+\mu^-$ for different values of input parameters showing the insensitivity on the number of KK-levels in summation (see Eq. 27 and Eq. 33).

IV.3 Electroweak precision constraints

Before we conclude, it would be relevant to discuss the constraints on the parameters coming from our analysis vis-a-vis electroweak data, which remains very instrumental in constraining any new-physics beyond the SM. Electroweak precision constraints on nmUED parameters have been discussed previously in [38, 39], while authors in ref. [13] restricts nmUED parameters from the consideration of Z -mass. However, in both of these cases nmUED action used for analysis are slightly different from that of ours. Ref. [38], while presenting their electroweak results used *equal* BLKT parameters for all the field along with a bulk mass term for the fermions. While the authors in the ref. [13], have considered several choices for the BLKT parameters. The case closest to our approach is where they have used equal BLKT parameters for Higgs and gauge bosons and set the BLKT parameter for the fermions equals to zero. Consequently, it would not be meaningful to directly apply the constraints derived in the above analysis to our case. So we have redone the analysis following the approaches of refs. [13, 38], however applied to our case.

In nmUED model, corrections to Peskin-Takeuchi parameters S , T and U as well as to Z mass appear through the correction to the Fermi constant, G_F at tree level, which is in stark contrast to the minimal version of the UED model where these correction appears through one loop processes. These quantities are modified by the correction of Fermi constant G_F which is determined from muon decay, i.e. a four-fermion process. The corrected Fermi constant G_F can be decomposed into two parts as:

$$G_F = G_F^0 + \delta G_F, \quad (40)$$

with G_F^0 is simply the contribution from W^\pm 0-mode exchange, while δG_F denotes the sum of the contributions from all non zero (even) W^\pm KK-modes. The effective Fermi constant can be expressed as the following.

$$G_F^0 = \frac{g_2^2}{4\sqrt{2}M_W^2}, \quad \delta G_F = \sum_{n \geq 2} \frac{g_2^2 (I_{n00}^G)^2}{4\sqrt{2}M_{W^{(n)}}^2}, \quad (41)$$

where,

$$\begin{aligned}
I_{n00}^G &= \sqrt{\pi R \left(1 + \frac{r_V}{\pi R}\right)} \int_0^{\pi R} dy [1 + r_f \{\delta(y) + \delta(y - \pi R)\}] a^n f_L^0 f_L^0, \\
&= \frac{\sqrt{\left(1 + \frac{r_V}{\pi R}\right)}}{\left(1 + \frac{r_f}{\pi R}\right)} \frac{\sqrt{2}}{\sqrt{1 + \frac{r_V^2 m_{V(n)}^2}{4} + \frac{r_V}{\pi R}}} \frac{(r_f - r_V)}{\pi R}.
\end{aligned} \tag{42}$$

A similar expression for δG_F has been presented in ref. [13]. The above expression for δG_F , agrees with the same in ref. [13] in the limit $r_f \rightarrow 0$.

Note that the above integral becomes zero when $r_f = r_V$, i.e., there is no correction of Fermi constant for this equality condition.

nmUED contributions to the S , T and U parameters can be written, following the approach of ref. [38, 39], as:

$$S_{\text{nmUED}} = 0, \quad T_{\text{nmUED}} = -\frac{1}{\alpha} \frac{\delta G_F}{G_F}, \quad U_{\text{nmUED}} = \frac{4 \sin^2 \theta_w}{\alpha} \frac{\delta G_F}{G_F}. \tag{43}$$

One can now compare the predictions from nmUED model with the experimental values given in the ref. [40]

$$S_{\text{NP}} = 0.05 \pm 0.11, \quad T_{\text{NP}} = 0.09 \pm 0.13, \quad U_{\text{NP}} = 0.01 \pm 0.11, \tag{44}$$

with input Higg mass $m_h = 125$ GeV and top quark mass $m_t = 173$ GeV. This would constrain the parameter space of nmUED model.

Before presenting the results of the above analysis, we would briefly discuss how δG_F modifies the Z -boson mass at the tree level [13]. This would be evident once we express the mass of Z -boson in terms of α , M_W and G_F : $M_Z = \frac{M_W \sqrt{\sqrt{2} G_F M_W^2}}{\sqrt{\sqrt{2} M_W^2 G_F - \pi \alpha}}$. The corrections to Z mass at tree level, in the framework of nmUED, would creep in through the corrected Fermi-constant, G_F . One can compare this with the so called tree level Z -mass defined by the relation $m_Z^{(expt)} - \delta^{(1-loop)} m_Z$ following the ref. [13]. Here, $\delta^{(1-loop)} m_Z$ stands for the 1-loop correction to the Z -boson mass in the SM.

We present our results in Fig. 8 (left panel) in terms of 95% C.L. lower limit on R^{-1} for several values of BLKT parameters. Region of the parameter space below a particular line has been ruled out from the consideration of T and U parameters. Furthermore, we have checked that the *tree level value* of Z -boson mass in the framework of nmUED, resides within the 95 % C.L. allowed tree level value [13] for the entire range of parameter space that we have considered in this work.

To compare the limits derived from our analysis ($B_s \rightarrow \mu^+ \mu^-$) with that from electroweak precision test, we present the allowed range of parameter space both from B_s decay and electroweak precision data, in $R_f - R^{-1}$ plane for six different choices of R_V in Fig. 8 (left panel).

In the right panel of Fig. 8, we present the allowed parameter space, on an expanded scale, only from the B_s decay analysis for sake of clarity. Each curve (in the left and right panel) corresponds to a particular value of R_V , each point of which represents a lower limit of R^{-1} in TeV corresponding to a particular value of R_f . So that the area under a particular curve has been dis-allowed by either from precision constraints or from $Br(B_s \rightarrow \mu^+\mu^-)$. It is evident from the plots that for a given value of R_V , higher values of R^{-1} are being ruled out from electroweak data for lower values of R_f , while B_s branching ratio would do better than the electroweak data in excluding values of R^{-1} for higher values of R_f . Finally, we mention while passing that the all of the parameter space (whether allowed or disallowed from electroweak data and B_s decay) is consistent with the Z -boson mass following the ref. [13].

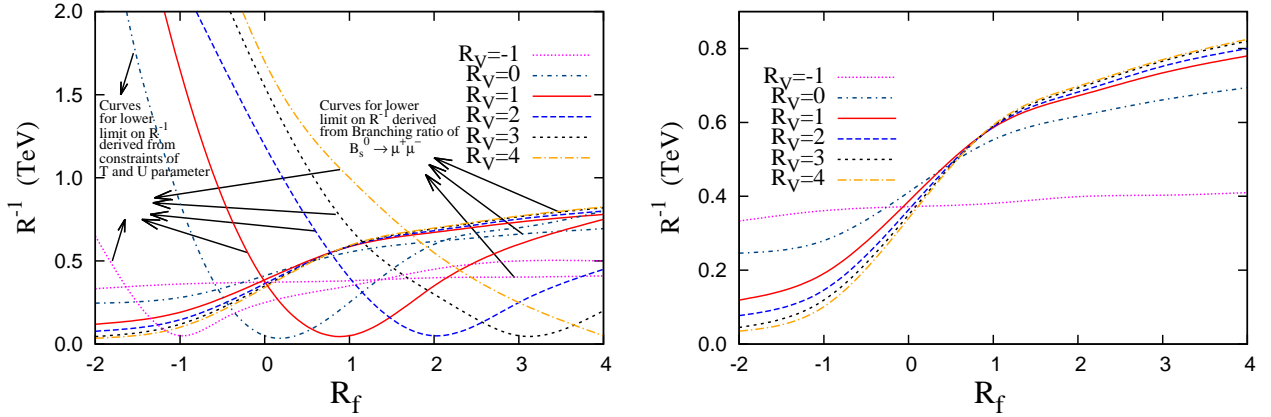


Figure 8: 95% C.L. exclusion contours in $R_f - R^{-1}$ plane for six different choices of R_V from branching ratio of $B_s \rightarrow \mu^+\mu^-$ decay and from constraints of T and U parameter. The area below a particular curve (fixed R_V) has been excluded at 95% C.L.

It has been evident from our analysis that the lower bounds on R^{-1} derived with negative values of BLKT parameters are not very interesting and the above values of R^{-1} have been already excluded from the consideration of electroweak data, which can be seen from the left panel of Fig. 8. The weak nature of the bounds on R^{-1} derived from $B_s \rightarrow \mu^+\mu^-$ branching ratio for negative values of BLT parameters, could be accounted by the higher masses of the KK-excitations, diminishing the contributions of penguins and boxes to the total decay amplitude. Furthermore, we have restricted our choice of BLT parameters upto 4. A careful look at the left or right panel of Fig. 8 (or Table 2), tells us that lower limits on R^{-1} are weakly sensitive to the values of R_V . So we expect that higher values of R_V would keep the lower limit on R^{-1} in the same ballpark.

V Conclusion

We have calculated the contribution of KK-excitations in the framework of non-minimal Universal Extra Dimensional model to the branching ratio of $B_{s(d)} \rightarrow \mu^+\mu^-$ at one loop level. Non-minimal UED is hallmarked by the presence of boundary localised kinetic and Yukawa terms along with an SM like action and field content however defined in a $4 + 1$ dimensional bulk. Boundary localised terms parametrise the unknown radiative corrections to the masses and couplings in the full 5-D theory. Presence of boundary terms modify the couplings and mass spectrum of KK-modes in the 4-D effective theory in a non-trivial manner.

To put our discussion into a context, we must remind that in UED, masses of the n^{th} KK-modes are nR^{-1} (R^{-1} being the compactification scale). Interactions among the different KK-excitations are very similar to their SM (0-modes) counterparts. However inclusion of BLT parameters would shift the masses of KK-modes from their UED values. For keeping our analysis simple we stick to the case of two different BLT parameters. The first one r_V , specifies the gauge and Higgs BLTs while the second one, r_f stands for equal fermion and Yukawa BLT coefficients.

Effective interaction for $B_{s(d)}$ meson decaying to a pair of $\mu^+\mu^-$ can be parametrised by a 4-fermion interaction. The coefficient for this effective interaction is calculable in the framework of SM and in the model of our interest namely the UED model. There are two sets of diagrams contributing to this decay process. The Z -penguins contribute dominantly while the box diagrams are sub-dominant. Diagrams 3, 4, 6, 7 and 8 in Fig. 2 and Ib and IIb of Fig. 3 captures the effects of top-Yukawa couplings, due to which this one loop mediated process is being amplified.

We have listed the amplitudes from each diagram separately in Appendix A and B. The total contribution coming from the penguins are finite and GIM mechanism plays a crucial role to tame the divergences. It should be noted that the final results is sum of contributions coming from different KK-levels and it also contains the SM contribution (i.e. from 0^{th} KK-mode). While summing over the KK-levels we restrict ourselves to 5 levels in view of a recent analysis relating the Higgs boson mass and cut-off of a UED theory [29]. It has been shown explicitly that the limits on the parameters derived from our analysis would change a little if we take 20 KK-levels in the summation instead of 5.

There is a one (two)-standard deviation difference between the experimentally measured branching ratio of $B_{s(d)} \rightarrow \mu^+\mu^-$ with its SM prediction. We have used the experimental data on the measured value of branching ratio of $B_{s(d)} \rightarrow \mu^+\mu^-$ to constrain the parameter space of nmUED model. As our calculation would reproduce the results of $Br(B_s \rightarrow \mu^+\mu^-)$ in the vanishing BLKT limits, at the very outset, we have used the above algorithm to set a lower limit on R^{-1} in the framework of UED. In case of UED, present analysis constrained R^{-1} to greater than 450 GeV at 95 % C.L. This limit in the framework of UED, is not one of the most stringent. However, this is in the same ballpark with the limits those are obtained from the consideration of R_b [18] or ρ -parameters [32]. The nmUED model has more than one parameters apart from the compactification radius. The BLT coefficients control the masses of KK-modes and their

interactions. So in the nmUED framework, any lower limit on R^{-1} would depend on these BLT coefficients. As for example, for $R_f = R_V = 3$, $R^{-1} > 0.7$ TeV, while for $R_f = 4$, $R_V = 3$, $R^{-1} > 0.8$ TeV. These lower limits on R^{-1} are so far the most stringent one in the framework of nmUED. Thus the recent experimental result of B_s meson decay to $\mu^+\mu^-$, combined with present analysis has excluded the largest region in the nmUED parameter space. Unfortunately the bounds on the parameters using the $Br(B_d \rightarrow \mu^+\mu^-)$ is not so competitive. Lower limits on R^{-1} derived from our analysis for negative values of R_f are not so stringent and the have been already ruled out from the consideration of electroweak precision data.

We have also reviewed the effect of electroweak precision constraint on nmUED parameter space. Our analysis reveals that the experimental data on the $B_s \rightarrow \mu^+\mu^-$ branching ratio would put more severe constraint on the lower limit of R^{-1} for positive values of R_f than the electroweak precision data.

Acknowledgements AD is partially supported by DAE-BRNS research project. AS acknowledges financial support from UGC in form of a Senior Research Fellowship. Authors are grateful to Sreerup Raychaudhury for taking part in the initial stage and many useful discussion.

References

- [1] G. Servant and T. M. P. Tait, New J. Phys. **4** (2002) 99, [arXiv: hep-ph/0209262]; G. Servant and T. M. P. Tait, Nucl. Phys. B **650** (2003) 391, [arXiv: hep-ph/0206071]; H. C. Cheng, J. L. Feng and K. T. Matchev, Phys. Rev. Lett. **89** (2002) 211301, [arXiv:hep-ph/0207125]; D. Majumdar, Phys. Rev. D **67** (2003) 095010, [arXiv:hep-ph/0209277]; F. Burnell and G. D. Kribs, Phys. Rev. D **73** (2006) 015001, [arXiv:hep-ph/0509118]; K. Kong and K. T. Matchev, JHEP **0601** (2006) 038 [arXiv:hep-ph/0509119]; M. Kakizaki, S. Matsumoto and M. Senami, Phys. Rev. D **74** (2006) 023504, [arXiv:hep-ph/0605280].
- [2] G. Belanger, M. Kakizaki and A. Pukhov, JCAP **1102** (2011) 009, [arXiv:1012.2577 [hep-ph]].
- [3] K. R. Dienes, E. Dudas and T. Gherghetta, Phys. Lett. B **436** (1998) 55, [arXiv:hep-ph/9803466]; K. Dienes, E. Dudas, and T. Gherghetta, Nucl. Phys. B **537** (1999) 47, [arXiv:hep-ph/9806292]; G. Bhattacharyya, A. Datta, S. K. Majee and A. Raychaudhuri, Nucl. Phys. B **760** (2007) 117, [arXiv:hep-ph/0608208].
- [4] K. Yoshioka, Mod. Phys. Lett. A **15** (2000) 29, [arXiv:hep-ph/9904433]; P. R. Archer, JHEP **09** (2012) 095 [arXiv:1204.4730 [hep-ph]].
- [5] T. Appelquist, H. C. Cheng and B. A. Dobrescu, Phys. Rev. D **64** (2001) 035002, [arXiv:hep-ph/0012100].
- [6] H. Georgi, A. K. Grant and G. Hailu, Phys. Lett. B **506** (2001) 207, [arXiv:hep-ph/0012379].

- [7] H. C. Cheng, K. T. Matchev and M. Schmaltz, Phys. Rev. D **66** (2002) 036005, [arXiv:hep-ph/0204342].
- [8] G. R. Dvali, G. Gabadadze, M. Kolanovic and F. Nitti, Phys. Rev. D **64** (2001) 084004, [arXiv:hep-ph/0102216].
- [9] M. S. Carena, T. M. P. Tait and C. E. M. Wagner, Acta Phys. Polon. B **33** (2002) 2355, [arXiv:hep-ph/0207056].
- [10] F. del Aguila, M. Perez Victoria and J. Santiago, JHEP **0302** (2003) 051, [arXiv:hep-th/0302023]; F. del Aguila, M. Perez Victoria and J. Santiago, [arXiv:hep-ph/0305119].
- [11] F. del Aguila, M. Perez-Victoria and J. Santiago, Acta Phys. Polon. B **34** (2003) 5511, [arXiv:hep-ph/0310353].
- [12] C. Schwinn, Phys. Rev. D **69** (2004) 116005, [arXiv:hep-ph/0402118].
- [13] T. Flacke, A. Menon and D. J. Phalen, Phys. Rev. D **79** (2009) 056009, [arXiv:0811.1598 [hep-ph]].
- [14] A. Datta, U. K. Dey, A. Shaw and A. Raychaudhuri, Phys. Rev. D **87** (2013) 076002, [arXiv:1205.4334 [hep-ph]].
- [15] T. Flacke, K. Kong and S. C. Park, Phys. Lett. B **728** (2014) 262, [arXiv:1309.7077 [hep-ph]].
- [16] J. Bonnevier, H. Melbeus, A. Merle and T. Ohlsson, Phys. Rev. D **85** (2012) 043524, [arXiv:1104.1430 [hep-ph]].
- [17] A. Datta, U. K. Dey, A. Raychaudhuri and A. Shaw, Phys. Rev. D **88** (2013) 016011, [arXiv:1305.4507 [hep-ph]].
- [18] T. Jha and A. Datta, JHEP **1503** (2015) 012, [arXiv:1410.5098 [hep-ph]].
- [19] U. K. Dey and T. S. Roy, Phys. Rev. D **88** (2013) 056016, [arXiv:1305.1016 [hep-ph]].
- [20] A. Datta, K. Nishiwaki and S. Niyogi, JHEP **1211** (2012) 154, [arXiv:1206.3987 [hep-ph]], A. Datta, K. Nishiwaki and S. Niyogi, JHEP **1401** (2014) 104, [arXiv:1310.6994 [hep-ph]].
- [21] A. Datta, A. Raychaudhuri and A. Shaw, Phys. Lett. B **730** (2014) 42, [arXiv:1310.2021 [hep-ph]]; A. Shaw, Eur. Phys. J. C **75** (2015) 33, [arXiv:1405.3139 [hep-ph]].
- [22] S. Chatrchyan et al, CMS Collaboration, Phys. Rev. Lett, **111** (2013) 101804, [arXiv:1307.5025[hep-ex]].
- [23] R. Aaij et al, LHCb Collaboration, Phys. Rev. Lett, **111** (2013) 101805, [arXiv:1307.5024[hep-ex]].
- [24] C. Bobeth, et al. Phys. Rev. Lett, **112** (2014) 101801, [arXiv:1311.0903[hep-ph]].

- [25] A. J. Buras, M. Spranger and A. Weiler, Nucl. Phys. B **660** (2003) 225, [arXiv:hep-ph/0212143].
- [26] A. Datta and A. Shaw, [arXiv:1408.0635 [hep-ph]].
- [27] Nature **522** (2015) 68, [arXiv:1411.4413[hep-ex]].
- [28] K. A. Olive et al. (Particle Data Group), Chin. Phys. C, **38** (2014) 090001.
- [29] A. Datta and S. Raychaudhuri, Phys. Rev. D **87** (2013) 035018, [arXiv:1207.0476 [hep-ph]].
- [30] G. Bhattacharyya and P. Dey, Phys. Rev. D **70** (2004) 116012, [arXiv:hep-ph/0407314].
- [31] P. Nath, M. Yamaguchi, Phys. Rev. D **60** (1999) 116006, [arXiv:hep-ph/9903298].
- [32] T. Appelquist and H. U. Yee, Phys. Rev. D **67** (2003) 055002, [arXiv:hep-ph/0211023].
- [33] A. J. Buras, A. Poschenrieder, M. Spranger and A. Weiler, Nucl. Phys. B **678** (2004) 455, [arXiv:hep-ph/0306158].
- [34] K. Agashe, N. G. Deshpande and G. H. Wu, Phys. Lett. B **514** (2001) 309, [arXiv:hep-ph/0105084]; D. Chakraverty, K. Huitu and A. Kundu, Phys. Lett. B **558** (2003) 173, [arXiv:hep-ph/0212047].
- [35] A. Strumia, Phys. Lett. B **466** (1999) 107, [arXiv:hep-ph/9906266]; T. G. Rizzo and J. D. Wells, Phys. Rev. D **61** (2000) 016007, [arXiv:hep-ph/9906234]; C. D. Carone, Phys. Rev. D **61** (2000) 015008, [arXiv:hep-ph/9907362].
- [36] U. Haisch and A. Weiler, Phys. Rev. D **76** (2007), 034014, [arXiv:hep-ph/0703064].
- [37] A. Belyaev, M. Brown, J. M. Moreno and C. Papineau, JHEP **1306** (2013) 080, [arXiv:1212.4858 [hep-ph]].
- [38] T. Flacke, K. Kong and S.C. Park, JHEP **05** (2013) 111 [arXiv:1303.0872].
- [39] T. Flacke and C. Pasold, Phys. Rev. D **85** (2012) 126007 [arXiv:1111.7250].
- [40] M. Baak et al, (for the Gfitter group), Eur. Phys. J. C **74** (2014) 3046, [arXiv:1407.3792 [hep-ph]].

Appendices

A Different contributions to Z-penguin and self-energy diagrams

The contributions of the Z-penguin diagrams to the functions C_n in Fig. 2 are given as follows:

$$F_1(x_{f(n)}) = \frac{1}{8} \left(c_{fn}^4 + s_{fn}^4 - \frac{4}{3} s_w^2 \right) \left[\Delta + \ln \frac{\mu^2}{M_{f(n)}^2} - \frac{3}{2} + h_q(x_{f(n)}) - 2x_{f(n)} h_q(x_{f(n)}) \right] (I_1^n)^2, \quad (\text{A-1})$$

$$F_2(x_{f(n)}) = \frac{1}{4} c_{fn}^2 s_{fn}^2 \left[\Delta + \ln \frac{\mu^2}{M_{f(n)}^2} - \frac{3}{2} + h_q(x_{f(n)}) + 2x_{f(n)} h_q(x_{f(n)}) \right] (I_1^n)^2, \quad (\text{A-2})$$

$$F_3(x_{f(n)}) = \frac{1}{16 M_{W(n)}^2} \left[\left((m_1^{(f)})^2 + (m_3^{(f)})^2 \right) \left(c_{fn}^2 - \frac{4}{3} s_w^2 \right) + \left((m_2^{(f)})^2 + (m_4^{(f)})^2 \right) \left(s_{fn}^2 - \frac{4}{3} s_w^2 \right) \right] \times \left[\Delta + \ln \frac{\mu^2}{M_{f(n)}^2} - \frac{1}{2} + h_q(x_{f(n)}) - 2x_{f(n)} h_q(x_{f(n)}) \right], \quad (\text{A-3})$$

$$F_4(x_{f(n)}) = -\frac{1}{8 M_{W(n)}^2} \left(m_1^{(f)} m_2^{(f)} + m_3^{(f)} m_4^{(f)} \right) c_{fn} s_{fn} \times \left[\Delta + \ln \frac{\mu^2}{M_{f(n)}^2} - \frac{1}{2} + h_q(x_{f(n)}) + 2x_{f(n)} h_q(x_{f(n)}) \right], \quad (\text{A-4})$$

$$F_5(x_{f(n)}) = -\frac{3}{4} c_w^2 \left[\Delta + \ln \frac{\mu^2}{M_{W(n)}^2} - \frac{1}{6} - x_{f(n)} h_w(x_{f(n)}) \right] (I_1^n)^2, \quad (\text{A-5})$$

$$F_6(x_{f(n)}) = -\frac{1}{16 M_{W(n)}^4} \left[\left((1 - 2 s_w^2) M_W^2 + 2 c_w^2 m_{V(n)}^2 \right) \left((m_1^{(f)})^2 + (m_2^{(f)})^2 \right) + \left((1 - 2 s_w^2) m_{V(n)}^2 + 2 c_w^2 M_W^2 \right) \left((m_3^{(f)})^2 + (m_4^{(f)})^2 \right) \right] \times \left[\Delta + \ln \frac{\mu^2}{M_{W(n)}^2} + \frac{1}{2} - x_{f(n)} h_w(x_{f(n)}) \right], \quad (\text{A-6})$$

$$F_7(x_{f(n)}) = \frac{M_W m_{V(n)}}{8 M_{W(n)}^4} \left(m_1^{(f)} m_3^{(f)} + m_2^{(f)} m_4^{(f)} \right) \left[\Delta + \ln \frac{\mu^2}{M_{W(n)}^2} + \frac{1}{2} - x_{f(n)} h_w(x_{f(n)}) \right], \quad (\text{A-7})$$

$$F_8(x_{f(n)}) = \frac{M_{f(n)}}{2 M_{W(n)}^4} \left[\left(s_w^2 M_W^2 - c_w^2 m_{V(n)}^2 \right) \left(m_1^{(f)} c_{fn} + m_2^{(f)} s_{fn} \right) + M_W m_{V(n)} \left(m_3^{(f)} c_{fn} + m_4^{(f)} s_{fn} \right) \right] h_w(x_{f(n)}) I_1^n, \quad (\text{A-8})$$

where the functions h_q and h_w are given by:

$$h_q(x) = \frac{1}{1-x} + \frac{\ln x}{(1-x)^2}, \quad (\text{A-9})$$

$$h_w(x) = \frac{1}{1-x} + \frac{x \ln x}{(1-x)^2}. \quad (\text{A-10})$$

The contributions of the self-energy diagrams to the functions C_n are given by the following expressions which are generated from Fig. 3:

$$\Delta S_1(x_{f(n)}) = \frac{1}{4} \left[\Delta - \frac{1}{2} \left\{ \frac{1+x_{f(n)}}{1-x_{f(n)}} + \frac{2x_{f(n)}^2 \ln x_{f(n)}}{(1-x_{f(n)})^2} \right\} - \ln \frac{M_{W(n)}^2}{\mu^2} \right] (I_1^n)^2, \quad (\text{A-11})$$

$$\Delta S_2(x_{f(n)}) = \frac{1}{8} [(I_2^n)^2 + (I_1^n)^2 x_f] \left[\Delta + \frac{1}{2} \left\{ \frac{1-3x_{f(n)}}{1-x_{f(n)}} - \frac{2x_{f(n)}^2 \ln x_{f(n)}}{(1-x_{f(n)})^2} \right\} - \ln \frac{M_{W(n)}^2}{\mu^2} \right]. \quad (\text{A-12})$$

Here $\Delta = \frac{2}{\epsilon} + \ln 4\pi - \gamma_E$, $D = 4 - \epsilon$.

B Different contributions to box diagrams

The contributions of the box diagrams to the functions B_n in Fig. 4 are given as follows:

$$H_{WW(n)} = -\frac{1}{4} \frac{M_W^2}{M_{W(n)}^2} U(x_{f(n)}, x_{\nu(n)}) (I_1^n)^4, \quad (\text{B-1})$$

$$H_{WG(n)} = \frac{1}{2} \frac{M_W^2 M_{f(n)} m_{\nu(n)}}{M_{W(n)}^6} \left[m_1^{(f)} c_{f(n)} + m_2^{(f)} s_{f(n)} \right] m_1^{(\nu)} \tilde{U}(x_{f(n)}, x_{\nu(n)}) (I_1^n)^2, \quad (\text{B-2})$$

$$H_{WH(n)} = \frac{1}{2} \frac{M_W^2 M_{f(n)} m_{\nu(n)}}{M_{W(n)}^6} \left[m_3^{(f)} c_{f(n)} + m_4^{(f)} s_{f(n)} \right] m_3^{(\nu)} \tilde{U}(x_{f(n)}, x_{\nu(n)}) (I_1^n)^2, \quad (\text{B-3})$$

$$H_{GH(n)} = -\frac{1}{8} \frac{M_W^2}{M_{W(n)}^6} \left[m_1^{(f)} m_3^{(f)} + m_2^{(f)} m_4^{(f)} \right] m_1^{(\nu)} m_3^{(\nu)} U(x_{f(n)}, x_{\nu(n)}), \quad (\text{B-4})$$

$$H_{GG(n)} = -\frac{1}{16} \frac{M_W^2}{M_{W(n)}^6} \left[(m_1^{(f)})^2 + (m_2^{(f)})^2 \right] (m_1^{(\nu)})^2 U(x_{f(n)}, x_{\nu(n)}), \quad (\text{B-5})$$

$$H_{HH(n)} = -\frac{1}{16} \frac{M_W^2}{M_{W(n)}^6} \left[(m_3^{(f)})^2 + (m_4^{(f)})^2 \right] (m_3^{(\nu)})^2 U(x_{f(n)}, x_{\nu(n)}). \quad (\text{B-6})$$

The functions U and \tilde{U} are defined as,

$$U(x_t, x_u) = \frac{x_t^2 \log x_t}{(x_t - x_u)(1 - x_t)^2} + \frac{x_u^2 \log x_u}{(x_u - x_t)(1 - x_u)^2} + \frac{1}{(1 - x_u)(1 - x_t)}, \quad (\text{B-7})$$

$$\tilde{U}(x_t, x_u) = \frac{x_t \log x_t}{(x_t - x_u)(1 - x_t)^2} + \frac{x_u \log x_u}{(x_u - x_t)(1 - x_u)^2} + \frac{1}{(1 - x_u)(1 - x_t)}. \quad (\text{B-8})$$

C Feynman rules for $B_{s(d)} \rightarrow \mu^+ \mu^-$ in nmUED

The Feynman rules for the different vertices with the assumption that all momenta and fields are incoming.

1) $Z^\mu W^{\nu\pm} S^\mp$: $\frac{g_2}{c_w M_{W^{(n)}}} g_{\mu\nu} C$, where C is given by:

$$\begin{aligned} Z^\mu W^{(n)+} G^{(n)-} : C &= -s_w^2 M_W^2 + c_w^2 m_{V^{(n)}}^2, \\ Z^\mu W^{(n)-} G^{(n)+} : C &= s_w^2 M_W^2 - c_w^2 m_{V^{(n)}}^2, \\ Z^\mu W^{(n)+} H^{(n)-} : C &= -i M_W m_{V^{(n)}}, \\ Z^\mu W^{(n)-} H^{(n)+} : C &= i M_W m_{V^{(n)}}. \end{aligned} \tag{C-1}$$

2) $Z^\mu S_1^\pm S_2^\mp$: $\frac{i g_2}{2 c_w M_{W^{(n)}}^2} (k_2 - k_1)_\mu C$, where C is given by:

$$\begin{aligned} Z^\mu G^{(n)+} G^{(n)-} : C &= -(c_w^2 - s_w^2) M_W^2 - 2c_w^2 m_{V^{(n)}}^2, \\ Z^\mu H^{(n)+} H^{(n)-} : C &= -2c_w^2 M_W^2 - (c_w^2 - s_w^2) m_{V^{(n)}}^2, \\ Z^\mu G^{(n)+} H^{(n)-} : C &= i M_W m_{V^{(n)}}, \\ Z^\mu G^{(n)-} H^{(n)+} : C &= -i M_W m_{V^{(n)}}. \end{aligned} \tag{C-2}$$

Here the scalar fields $S \equiv H, G$.

3) $Z^\mu(k_1) W^{\nu+}(k_2) W^{\lambda-}(k_3)$:

$$i g_2 c_w [g_{\mu\nu}(k_2 - k_1)_\lambda + g_{\mu\lambda}(k_1 - k_3)_\nu + g_{\lambda\nu}(k_3 - k_2)_\mu]. \tag{C-3}$$

4) $Z^\mu \bar{f}_1 f_2$: $\frac{i g_2}{6 c_w} \gamma_\mu (P_L C_L + P_R C_R)$, where C_L and C_R are given by:

$$\begin{aligned} Z^\mu \bar{u}_i u_i : \quad & \begin{cases} C_L = 3 - 4s_w^2, \\ C_R = -4s_w^2, \end{cases} & Z^\mu \bar{d}_j d_j : \quad & \begin{cases} C_L = -3 + 2s_w^2, \\ C_R = 2s_w^2, \end{cases} \\ Z^\mu \bar{\nu}_i \nu_i : \quad & \begin{cases} C_L = 3, \\ C_R = 0, \end{cases} & Z^\mu \bar{e}_j e_j : \quad & \begin{cases} C_L = -3 + 6s_w^2, \\ C_R = 6s_w^2, \end{cases} \\ Z^\mu \bar{T}_i^{1(n)} T_i^{1(n)} : \quad & \begin{cases} C_L = -4s_w^2 + 3c_{in}^2, \\ C_R = -4s_w^2 + 3c_{in}^2, \end{cases} & Z^\mu \bar{T}_i^{2(n)} T_i^{2(n)} : \quad & \begin{cases} C_L = -4s_w^2 + 3s_{in}^2, \\ C_R = -4s_w^2 + 3s_{in}^2, \end{cases} \\ Z^\mu \bar{T}_i^{1(n)} T_i^{2(n)} : \quad & \begin{cases} C_L = -3s_{in}c_{in}, \\ C_R = 3s_{in}c_{in}, \end{cases} & Z^\mu \bar{T}_i^{2(n)} T_i^{1(n)} : \quad & \begin{cases} C_L = -3s_{in}c_{in}, \\ C_R = 3s_{in}c_{in}. \end{cases} \end{aligned} \tag{C-4}$$

5) $S^\pm \bar{f}_1 f_2 = \frac{g_2}{\sqrt{2} M_{W^{(n)}}} (P_L C_L + P_R C_R)$, where C_L and C_R are given by:

$$\begin{aligned}
G^+ \bar{u}_i d_j : & \quad \begin{cases} C_L = -m_i V_{ij}, \\ C_R = m_j V_{ij}, \end{cases} & G^- \bar{d}_j u_i : & \quad \begin{cases} C_L = -m_j V_{ij}^*, \\ C_R = m_i V_{ij}^*, \end{cases} \\
G^{(n)+} \bar{T}_i^{1(n)} d_j : & \quad \begin{cases} C_L = -m_1^{(i)} V_{ij}, \\ C_R = M_1^{(i,j)} V_{ij}, \end{cases} & G^{(n)-} \bar{d}_j T_i^{1(n)} : & \quad \begin{cases} C_L = -M_1^{(i,j)} V_{ij}^*, \\ C_R = m_1^{(i)} V_{ij}^*, \end{cases} \\
G^{(n)+} \bar{T}_i^{2(n)} d_j : & \quad \begin{cases} C_L = m_2^{(i)} V_{ij}, \\ C_R = -M_2^{(i,j)} V_{ij}, \end{cases} & G^{(n)-} \bar{d}_j T_i^{2(n)} : & \quad \begin{cases} C_L = M_2^{(i,j)} V_{ij}^*, \\ C_R = -m_2^{(i)} V_{ij}^*, \end{cases} \\
G^+ \bar{\nu}_i e_j : & \quad \begin{cases} C_L = 0, \\ C_R = m_j \delta_{ij}, \end{cases} & G^- \bar{e}_j \nu_i : & \quad \begin{cases} C_L = -m_j \delta_{ij}, \\ C_R = 0, \end{cases} \\
G^{(n)+} \bar{\nu}_i \mathcal{L}_j^{(n)} : & \quad \begin{cases} C_L = 0, \\ C_R = m_1^{(j)} \delta_{ij}, \end{cases} & G^{(n)-} \bar{\mathcal{L}}_j^{(n)} \nu_i : & \quad \begin{cases} C_L = -m_1^{(j)} \delta_{ij}, \\ C_R = 0, \end{cases} \\
G^{(n)+} \bar{\nu}_i \mathcal{E}_j^{(n)} : & \quad \begin{cases} C_L = 0, \\ C_R = -m_2^{(j)} \delta_{ij}, \end{cases} & G^{(n)-} \bar{\mathcal{E}}_j^{(n)} \nu_i : & \quad \begin{cases} C_L = m_2^{(j)} \delta_{ij}, \\ C_R = 0, \end{cases} \\
H^{(n)+} \bar{T}_i^{1(n)} d_j : & \quad \begin{cases} C_L = -m_3^{(i)} V_{ij}, \\ C_R = M_3^{(i,j)} V_{ij}, \end{cases} & H^{(n)-} \bar{d}_j T_i^{1(n)} : & \quad \begin{cases} C_L = -M_3^{(i,j)} V_{ij}^*, \\ C_R = m_3^{(i)} V_{ij}^*, \end{cases} \\
H^{(n)+} \bar{T}_i^{2(n)} d_j : & \quad \begin{cases} C_L = m_4^{(i)} V_{ij}, \\ C_R = -M_4^{(i,j)} V_{ij}, \end{cases} & H^{(n)-} \bar{d}_j T_i^{2(n)} : & \quad \begin{cases} C_L = M_4^{(i,j)} V_{ij}^*, \\ C_R = -m_4^{(i)} V_{ij}^*, \end{cases} \\
H^{(n)+} \bar{\nu}_i \mathcal{L}_j^{(n)} : & \quad \begin{cases} C_L = 0, \\ C_R = m_3^{(j)} \delta_{ij}, \end{cases} & H^{(n)-} \bar{\mathcal{L}}_j^{(n)} \nu_i : & \quad \begin{cases} C_L = -m_3^{(j)} \delta_{ij}, \\ C_R = 0, \end{cases} \\
H^{(n)+} \bar{\nu}_i \mathcal{E}_j^{(n)} : & \quad \begin{cases} C_L = 0, \\ C_R = -m_4^{(j)} \delta_{ij}, \end{cases} & H^{(n)-} \bar{\mathcal{E}}_j^{(n)} \nu_i : & \quad \begin{cases} C_L = m_4^{(j)} \delta_{ij}, \\ C_R = 0, \end{cases}
\end{aligned} \tag{C-5}$$

Here the fermion fields $f \equiv u, d, T_t^1, T_t^2, \nu, e, \mathcal{L}_\nu, \mathcal{L}_e, \mathcal{E}$.

6) $W^{\mu\pm} \bar{f}_1 f_2 : \frac{ig_2}{\sqrt{2}} \gamma_\mu P_L C_L$, where C_L is given by:

$$\begin{aligned}
W^{\mu+} \bar{u}_i d_j : & \quad C_L = V_{ij}, & W^{\mu-} \bar{d}_j u_i : & \quad C_L = V_{ij}^*, \\
W^{\mu(n)+} \bar{T}_i^{1(n)} d_j : & \quad C_L = I_1^n c_{in} V_{ij}, & W^{\mu(n)-} \bar{d}_j T_i^{1(n)} : & \quad C_L = I_1^n c_{in} V_{ij}^*, \\
W^{\mu(n)+} \bar{T}_i^{2(n)} d_j : & \quad C_L = -I_1^n s_{in} V_{ij}, & W^{\mu(n)-} \bar{d}_j T_i^{2(n)} : & \quad C_L = -I_1^n s_{in} V_{ij}^*, \\
W^{\mu+} \bar{\nu}_i e_j : & \quad C_L = \delta_{ij}, & W^{\mu-} \bar{e}_j \nu_i : & \quad C_L = \delta_{ij}, \\
W^{\mu(n)+} \bar{\nu}_i \mathcal{L}_j^{(n)} : & \quad C_L = I_1^n \delta_{ij}, & W^{\mu(n)-} \bar{\mathcal{L}}_j^{(n)} \nu_i : & \quad C_L = I_1^n \delta_{ij}, \\
W^{\mu(n)+} \bar{\nu}_i \mathcal{E}_j^{(n)} : & \quad C_L = 0, & W^{\mu(n)-} \bar{\mathcal{E}}_j^{(n)} \nu_i : & \quad C_L = 0.
\end{aligned} \tag{C-6}$$

The mass parameters $m_x^{(i)}$ are given by:

$$\begin{aligned}
m_1^{(i)} &= I_2^n m_{V^{(n)}} c_{in} + I_1^n m_i s_{in}, \\
m_2^{(i)} &= -I_2^n m_{V^{(n)}} s_{in} + I_1^n m_i c_{in}, \\
m_3^{(i)} &= -I_2^n i M_W c_{in} + I_1^n i \frac{m_{V^{(n)}} m_i}{M_W} s_{in}, \\
m_4^{(i)} &= I_2^n i M_W s_{in} + I_1^n i \frac{m_{V^{(n)}} m_i}{M_W} c_{in},
\end{aligned} \tag{C-7}$$

where m_i represents the mass of the 0-mode *up-type* fermion and $c_{in} = \cos(\alpha_{in})$ and $s_{in} = \sin(\alpha_{in})$ with α_{in} as defined earlier.

And the mass parameters $M_x^{(i,j)}$ are:

$$\begin{aligned}
M_1^{(i,j)} &= I_1^n m_j c_{in}, \\
M_2^{(i,j)} &= I_1^n m_j s_{in}, \\
M_3^{(i,j)} &= I_1^n i \frac{m_{V^{(n)}} m_j}{M_W} c_{in}, \\
M_4^{(i,j)} &= I_1^n i \frac{m_{V^{(n)}} m_j}{M_W} s_{in},
\end{aligned} \tag{C-8}$$

where m_j represents the mass of the 0-mode *down-type* fermion. Here, I_1^n and I_2^n are the overlap integrals given in Eqs. 23 and 24 respectively.